Journal of Mathematical Modeling
Vol. -, No. -, 2026, pp. -. Research Article

JMM

Numerical analysis for a parameter-uniform scheme of a special class of two-parameter singularly perturbed 2D convection-diffusion systems

Harini Chandrasekaran, Vembu Shanthi*

Department of Mathematics, National Institute of Technology, Tiruchirappalli - 620015, Tamil Nadu, India.

Email(s): cgharini55555@gmail.com, vshanthi@nitt.edu

Abstract. This paper considers a class of weakly coupled two-parameter singularly perturbed convection-diffusion systems whose solutions exhibit exponential, characteristic, and corner layers driven by the two distinct perturbation parameters. To resolve these multiscale features effectively and suppress non-physical oscillations, an upwind finite difference scheme is developed on a piecewise-uniform Shishkin mesh. The resulting discrete problem is shown to satisfy a discrete minimum principle, which establishes the stability of the numerical method. A detailed component-wise error analysis demonstrates that the proposed scheme is parameter-uniform. In particular, the method achieves a maximum pointwise error of $\mathcal{O}(N^{-1}\ln N)$ in the reaction-dominated regime and $\mathcal{O}(N^{-1}(\ln N)^2)$ in the anisotropic convection-dominated regime. Numerical experiments, in which the errors are estimated by the double-mesh principle, are presented; the computed errors and convergence rates are consistent with the theoretical estimates for all the perturbation parameters tested.

Keywords: Singularly perturbed system; two-parameter problem; characteristic layers; Shishkin mesh; finite difference scheme.
AMS Subject Classification 2010: 35B25, 35J57, 65N06, 65N12, 65N15, 65N50.

1 Introduction

In computational mechanics and applied mathematics, accurately resolving singularly perturbed problems remains a formidable challenge. These problems are defined by the presence of a small positive parameter, ε, multiplying the highest-order derivative in the governing equation, which introduces a severe scale difference into the model. This forces the solution to undergo abrupt, localized changes forming boundary or interior layers over very small spatial regions. Applying conventional numerical schemes on uniform grids typically fails to resolve these sharp transitions, generating severe artificial oscillations unless one utilizes a prohibitively dense mesh [21]. Therefore, contemporary research strongly emphasizes developing parameter-uniform numerical techniques capable of ensuring reliable approximations completely independent of how small the perturbation parameter becomes [5, 6, 8, 14, 18].

Within this domain, models governed by convection and diffusion are of particular interest due to their prevalence in transport-dominated systems. Although researchers have thoroughly established the one-dimensional

*Corresponding author
Received: 23 July 2026/ Revised: 18 November 2026/ Accepted: 19 November 2026
DOI: 10.22124/jmm.2026.34356.3168

© 2026 University of Guilan

Corrected Proof

theory for cases involving coupled dynamics or multiple perturbation parameters, extending this analysis to higher dimensions presents entirely new obstacles. Specifically, whenever the velocity field aligns parallel to a given boundary in a two-dimensional domain, specialized characteristic boundary layers emerge alongside the usual exponential ones. Because parabolic partial differential equations govern the flow inside these characteristic regions, their decay mechanisms and internal structures differ drastically from traditional exponential profiles.

Hemker's analysis of flow around a circular object motivated extensive research on characteristic boundary layers [13]. Subsequent studies focused on the numerical challenges associated with these layers. Kellogg and Stynes [15] successfully derived essential a priori derivative estimates for a constant-coefficient model problem on the unit square. Their theoretical bounds directly enabled O'Riordan and Shishkin [20] to formulate highly effective layer-adapted grid geometries. In related work, investigators adapted this methodology to handle complicated domain shapes, non-smooth boundary conditions, and specialized weak formulations [3, 7, 10, 11]. More recently, researchers adapted these foundational mesh principles to solve weakly coupled systems [2].

When a secondary perturbation parameter is introduced, the system develops heavily anisotropic layers because the competing convective and diffusive forces directly control the local width of the boundary transitions. While researchers have studied the numerical resolution of two-parameter problems featuring characteristic layers, finite element methods (FEM) dominate the current literature. Early FEM investigations utilized asymptotic expansions to build a foundational understanding of these dynamics [17]. Later, Teofanov and Roos [23] established a strict analytical decomposition of the solution and bounded its derivatives, allowing researchers to prove uniform convergence within the energy norm. Continued FEM research then branched into streamline-diffusion techniques, superconvergence behavior, and alternative specialized mesh topologies [1, 22].

While these finite element approaches have been extensively developed for scalar problems, and finite difference schemes have been applied to two-parameter coupled systems lacking characteristic boundary layers [4] and to two-parameter scalar problems with characteristic boundary layers [12], the extension to coupled models exhibiting both characteristic and regular boundary layers under two perturbation parameters presents distinct numerical challenges. The main contributions of this work, relative to these studies, are fourfold. First, the particular coefficient structure we analyze features convection acting along the x-direction only. This contrasts with the two-parameter weakly coupled system in [4], which includes convective terms in both directions and thereby produces only regular boundary layers. Our anisotropic convective behavior gives rise to characteristic boundary layers in the y-direction and regular boundary layers in the x-direction. Second, an explicit two-parameter regime classification captures how the ratio of the two perturbation parameters governs the solution behavior of the system. We demonstrate that the transverse characteristic layers remain structurally invariant, whereas the longitudinal boundary layers adapt dynamically to the transition between the reaction-dominated and convection-dominated regimes. Third, we establish a specific parameter-uniform upwind finite difference scheme on a tailored Shishkin mesh. Finally, we prove a parameter-uniform error estimate in the maximum norm, valid for every ratio of the two perturbation parameters. The bounds on the layer components follow the analysis of [12] for the scalar problem, which we extend to the weakly coupled system (see Section 2).

Now, let us consider the following singularly perturbed two-dimensional convection-diffusion system with two different parameters, defined on $\mathscr{D} = (0,1)\times(0,1)$,

$$\begin{aligned} &\mathscr{L}_{\varepsilon_1,\varepsilon_2}\bar{z}(x,y) \equiv \varepsilon_1\left(\frac{\partial^2\bar{z}}{\partial x^2}+\frac{\partial^2\bar{z}}{\partial y^2}\right)+\varepsilon_2\mathbf{P}(x,y)\frac{\partial\bar{z}}{\partial x}-\mathbf{Q}(x,y)\bar{z}=\bar{r}(x,y), \quad (x,y)\in\mathscr{D},\\ &\bar{z}(x,y)=\bar{0}, \quad (x,y)\in\mathscr{B}. \end{aligned} \tag{1}$$

In this setup, we define the unknown solution vector and the source term as $\bar{z}(x,y) = (z_1(x,y), z_2(x,y))^T$ and $\bar{r}(x,y) = (r_1(x,y), r_2(x,y))^T$. The coefficient matrices are given by $\mathbf{P}(x,y) = \mathrm{diag}(p_1(x,y), p_2(x,y))$ and $\mathbf{Q}(x,y) = \begin{pmatrix} q_{11}(x,y) & -q_{12}(x,y) \\ -q_{21}(x,y) & q_{22}(x,y) \end{pmatrix}$. The differential operator is denoted by $\mathscr{L}_{\varepsilon_1,\varepsilon_2}\bar{z} = (\mathscr{L}^1_{\varepsilon_1,\varepsilon_2}\bar{z}, \mathscr{L}^2_{\varepsilon_1,\varepsilon_2}\bar{z})^T$. Further, $\bar{\mathscr{D}} = [0,1]\times[0,1]$ represents the closure of the domain and the boundary is partitioned into $\mathscr{B} = \bigcup_{i=1}^{4}\mathscr{B}_i$, where

$$\mathscr{B}_1 = \{(x,y)\,|x=0, 0\le y\le 1\}, \quad \mathscr{B}_2 = \{(x,y)\,|0\le x\le 1, y=0\},$$

Corrected Proof

$$\mathscr{B}_3 = \{(x,y)\,|x = 1, 0 \le y \le 1\}, \quad \mathscr{B}_4 = \{(x,y)\,|0 \le x \le 1, y = 1\}.$$

The perturbation parameters ε_1 and ε_2 satisfy $0 < \varepsilon_1, \varepsilon_2 \ll 1$. Also, we suppose that the convective and the reaction coefficient functions satisfy:

$$\begin{aligned} &p_i(x,y) \ge \rho > 0, \quad q_{ij}(x,y) > 0, \quad i,j = 1,2, \\ &q_{ii}(x,y) - q_{ij}(x,y) \ge \gamma^2 > 0, \quad i,j = 1,2,\ i \ne j, \end{aligned} \tag{2}$$

for fixed positive constants ρ and γ that are independent of the perturbation parameters ε_1 and ε_2. Additionally, we assume there exists a positive constant ω, also independent of ε_1 and ε_2, such that $\omega < \min\left\{\frac{q_{11}-q_{12}}{2p_1}, \frac{q_{22}-q_{21}}{2p_2}\right\}$ [19]. These conditions ensure that $\mathbf{Q}(x,y)$ satisfies the diagonal-dominance properties, which are essential for the minimum principle. Furthermore, while the condition $r_i \in C^{1,\alpha}(\bar{\mathscr{D}})$ for some $\alpha \in (0,1)$, together with the corner condition $\bar{r} = \bar{0}$ stated below, is sufficient to guarantee the existence of a unique global solution $\bar{z} \in C^{3,\alpha}(\bar{\mathscr{D}})$ [9], the derivation of the parameter-uniform bounds on the higher-order derivatives of the layer components requires further regularity. Thus, we assume the coefficient and source functions are sufficiently smooth for the expansions in Section 2 and satisfy the first-order corner compatibility condition $\bar{r} = \bar{0}$ at the four vertices of $\bar{\mathscr{D}}$ [9, 20], which is condition (2.3) of [12] for zero boundary data. With the signs in (1), the flow is directed from $x = 1$ towards $x = 0$ (see Subsection 2.1).

Notation: Throughout this paper, standard mathematical font is used for scalar functions (e.g., $z_1(x,y)$), while boldface letters denote matrices (e.g., $\mathbf{P}(x,y)$). Variables with an overbar (e.g., $\bar{z}(x,y)$ and $\bar{Z}_{i,j}$) denote vector-valued continuous and discrete functions. For vector inequalities, the relation $u_i \le v_i$ for $i = 1,2$ is written compactly as $\bar{u} \le \bar{v}$. The maximum norm is denoted by $\|\cdot\|$, where for a vector $\bar{u} = (u_1, u_2)^T$, it is defined as $\|\bar{u}\| = \max\{\|u_1\|, \|u_2\|\}$. Finally, C denotes a generic positive constant independent of the mesh parameter N and the perturbation parameters ε_1 and ε_2, and $\bar{C} = (C,C)^T$ denotes the corresponding constant vector.

The subsequent sections are structured as follows. Section 2 formulates the underlying mathematical properties of the continuous system. Within this section, we establish the required stability results, formulate a minimum principle, and decompose the exact solution to extract specific bounds for each regular and singular component. Section 3 constructs the computational domain utilizing a piecewise-uniform Shishkin grid and defines the upwind numerical approximation on this discretized domain. Section 4 evaluates the local truncation errors and proves parameter-uniform convergence across all parameter ranges. Section 5 reports numerical experiments, with errors estimated by the double-mesh principle, which illustrate the theoretical bounds. Finally, Section 6 provides our concluding remarks.

2 Analytical perspectives on the continuous problem

This section presents the fundamental mathematical properties of the continuous system defined by (1)–(2). We establish a minimum principle, derive the corresponding stability results, and obtain derivative estimates for the exact solution.

Lemma 1 (Minimum principle)**.** *Let $\mathscr{L}_{\varepsilon_1,\varepsilon_2}$ be the differential operator defined in (1) satisfying the assumptions in (2). Suppose that $\bar{\phi} = (\phi_1, \phi_2)^T$ satisfies $\bar{\phi}(x,y) \ge \bar{0}$ on $\mathscr{B}$ and $\mathscr{L}_{\varepsilon_1,\varepsilon_2}\bar{\phi}(x,y) \le \bar{0}$ in $\mathscr{D}$. Then, $\forall (x,y) \in \bar{\mathscr{D}}$, $\bar{\phi}(x,y) \ge \bar{0}$.*

Proof. Assume, on the contrary, that $\bar{\phi}$ attains a negative minimum in $\bar{\mathscr{D}}$ at the point $(\hat{x},\hat{y})$. Without loss of generality, let the minimum occur in the first component, that is,

$$\phi_1(\hat{x},\hat{y}) = \min_{(x,y)\in\bar{\mathscr{D}}} \{\phi_1(x,y), \phi_2(x,y)\} < 0.$$

Corrected Proof

Consequently, we have $\phi_1(\hat{x},\hat{y}) \le \phi_2(\hat{x},\hat{y})$. Since $\bar{\phi}(x,y) \ge \bar{0}$ on $\mathscr{B}$, the point $(\hat{x},\hat{y}) \notin \mathscr{B}$. Hence, $(\hat{x},\hat{y}) \in \mathscr{D}$. As $\phi_1(\hat{x},\hat{y})$ is the minimum point, we have

$$\frac{\partial \phi_1}{\partial x}(\hat{x},\hat{y}) = \frac{\partial \phi_1}{\partial y}(\hat{x},\hat{y}) = 0, \quad \frac{\partial^2 \phi_1}{\partial x^2}(\hat{x},\hat{y}) \ge 0, \text{ and } \frac{\partial^2 \phi_1}{\partial y^2}(\hat{x},\hat{y}) \ge 0. \tag{3}$$

Using (2) and (3), we get

$$\begin{aligned}\mathscr{L}^1_{\varepsilon_1,\varepsilon_2}\bar{\phi}(\hat{x},\hat{y}) = \varepsilon_1 \left(\frac{\partial^2 \phi_1}{\partial x^2}(\hat{x},\hat{y}) + \frac{\partial^2 \phi_1}{\partial y^2}(\hat{x},\hat{y})\right) + \varepsilon_2 p_1(\hat{x},\hat{y}) \frac{\partial \phi_1}{\partial x}(\hat{x},\hat{y}) \\ - \left(q_{11}(\hat{x},\hat{y}) - q_{12}(\hat{x},\hat{y})\right) \phi_1(\hat{x},\hat{y}) + q_{12}(\hat{x},\hat{y}) \left(\phi_2(\hat{x},\hat{y}) - \phi_1(\hat{x},\hat{y})\right) > 0,\end{aligned}$$

which contradicts the hypothesis $\mathscr{L}_{\varepsilon_1,\varepsilon_2}\bar{\phi}(x,y) \le \bar{0}$ in $\mathscr{D}$. Therefore, $\bar{\phi}(x,y) \ge \bar{0}$, for all $(x,y) \in \bar{\mathscr{D}}$. □

Lemma 2 (Stability result)**.** *The solution $\bar{z}(x,y)$ of the problem (1)-(2) satisfies*

$$\|\bar{z}(x,y)\|_{\bar{\mathscr{D}}} \le \max_{(x,y)\in\mathscr{B}} \{\|\bar{z}(x,y)\|\} + \frac{1}{\gamma^2}\|\bar{r}(x,y)\|_{\bar{\mathscr{D}}}.$$

Proof. Consider the barrier function $\bar{\psi}^{\pm} = (\psi_1^{\pm}, \psi_2^{\pm})$ as,

$$\psi_i^{\pm}(x,y) = \alpha \pm z_i(x,y), \quad (x,y) \in \mathscr{D},$$

for $i = 1,2$ and $\alpha = \max_{\mathscr{B}} \{\|\bar{z}\|\} + \frac{1}{\gamma^2}\|\bar{r}\|_{\bar{\mathscr{D}}}$. Here we observe that $\bar{\psi}^{\pm}(x,y) \ge 0$, on $\mathscr{B}$ and, since $\mathscr{L}^i_{\varepsilon_1,\varepsilon_2}\bar{\psi}^{\pm} = -(q_{ii} - q_{ij})\alpha \pm r_i \le -\gamma^2\alpha + \|\bar{r}\|_{\bar{\mathscr{D}}} \le 0$, $\mathscr{L}_{\varepsilon_1,\varepsilon_2}\bar{\psi}^{\pm} \le 0$, in $\mathscr{D}$. Now, applying Lemma 1, we obtain $\bar{\psi}^{\pm}(x,y) \ge 0$, $\forall (x,y) \in \bar{\mathscr{D}}$ and this gives the required bound. □

Lemma 3. *Let $\bar{z}(x,y)$ be the solution of (1)-(2). Then, for $1 \le m+n \le 3$, we have*

$$\left\| \frac{\partial^{m+n}\bar{z}}{\partial x^m \partial y^n} \right\|_{\mathscr{D}} \le \begin{cases} C\varepsilon_1^{-(m+n)/2}, & \rho\varepsilon_2^2 < \omega\varepsilon_1, \\ C\left(\dfrac{\varepsilon_1}{\varepsilon_2}\right)^{-(m+n)}, & \rho\varepsilon_2^2 \ge \omega\varepsilon_1. \end{cases} \tag{4}$$

Proof. Based on the analytical arguments outlined in [2, 4, 18], we derive the parameter-explicit bounds by evaluating the continuous system in stretched coordinates tailored to each parameter regime.

Case (i): $\rho\varepsilon_2^2 < \omega\varepsilon_1$**.** We introduce the transformation $\nu = x/\sqrt{\varepsilon_1}$ and $\eta = y/\sqrt{\varepsilon_1}$, which maps the original domain $\mathscr{D}$ and its boundary $\mathscr{B}$ to $\mathscr{D}_\varepsilon = (0, 1/\sqrt{\varepsilon_1})^2$ and $\mathscr{B}_\varepsilon$, respectively. Let $\bar{z}_\varepsilon(\nu,\eta) = \bar{z}(x,y)$ denote the solution in these new variables, with the coefficient matrices and source term ($\mathbf{P}_\varepsilon$, $\mathbf{Q}_\varepsilon$, and $\bar{r}_\varepsilon$) defined analogously. Substituting this into the governing system (1) yields the transformed equation:

$$\left(\frac{\partial^2 \bar{z}_\varepsilon}{\partial \nu^2} + \frac{\partial^2 \bar{z}_\varepsilon}{\partial \eta^2}\right) + \frac{\varepsilon_2}{\sqrt{\varepsilon_1}}\mathbf{P}_\varepsilon(\nu,\eta)\frac{\partial \bar{z}_\varepsilon}{\partial \nu} - \mathbf{Q}_\varepsilon(\nu,\eta)\bar{z}_\varepsilon(\nu,\eta) = \bar{r}_\varepsilon(\nu,\eta).$$

In this transformed setting, the regime condition $\rho\varepsilon_2^2 < \omega\varepsilon_1$ gives $\frac{\varepsilon_2}{\sqrt{\varepsilon_1}} < \sqrt{\frac{\omega}{\rho}} \le C$. Consequently, the transformed operator is uniformly elliptic, its coefficients are bounded independently of ε_1 and ε_2, and the homogeneous boundary condition $\bar{z}_\varepsilon = \bar{0}$ on $\mathscr{B}_\varepsilon$ is preserved. Since the diffusion operator $\Delta_{\nu,\eta}\mathbf{I}$ and the convection operator $\mathbf{P}_\varepsilon \frac{\partial}{\partial \nu}$ are diagonal, the off-diagonal coupling terms in $\mathbf{Q}_\varepsilon \bar{z}_\varepsilon$ can be moved to the right-hand side. Hence the classical local *a priori* interior and boundary Schauder estimates [16, Chapter 3] apply to each component. Near the vertices of the square, where the boundary is not smooth, these estimates are replaced by the corner regularity results of [9], which apply because the data are smooth and $\bar{r} = \bar{0}$ at the vertices (Section 1). For $(\nu_0,\eta_0) \in \bar{\mathscr{D}}_\varepsilon$ and a fixed $\delta > 0$, let $N_\delta = (\nu_0 - \delta, \nu_0 + \delta) \times (\eta_0 - \delta, \eta_0 + \delta) \cap \bar{\mathscr{D}}_\varepsilon$, and define $N_{2\delta}$ with 2δ in place of δ. In the

Corrected Proof

$C^{3,\alpha}(\bar{N}_\delta)$ estimate for the component $z_{\varepsilon,i}$ of $\bar{z}_\varepsilon = (z_{\varepsilon,1}, z_{\varepsilon,2})^T$, the coupling term enters through the $C^{1,\alpha}(\bar{N}_{2\delta})$ norm of $z_{\varepsilon,j}$, $j \neq i$, which is bounded by $\|z_{\varepsilon,j}\|_{C^{2,\alpha}(\bar{N}_{2\delta})}$. By the interpolation inequality [16, Chapter 7, (5.7)], $\|z_{\varepsilon,j}\|_{C^{2,\alpha}(\bar{N}_{2\delta})} \leq \theta \|z_{\varepsilon,j}\|_{C^{3,\alpha}(\bar{N}_{2\delta})} + C_\theta \|z_{\varepsilon,j}\|$ for every $\theta > 0$. As in [16, Chapter 7, Section 5], we add the estimates for the two components and choose θ, depending only on the constant of the Schauder estimate, so small that these $C^{3,\alpha}$ terms are absorbed. This uses only the finiteness of the $C^{3,\alpha}$ norms, which holds since $\bar{z} \in C^{3,\alpha}(\bar{\mathscr{D}})$, and gives

$$\|\bar{z}_\varepsilon\|_{C^{3,\alpha}(\bar{N}_\delta)} \leq C\,(1 + \|\bar{z}_\varepsilon\|)\,,$$

where C depends only on δ, α, the data and the Hölder norms of the coefficients. These norms are bounded independently of ε_1 and ε_2, since $\varepsilon_2/\sqrt{\varepsilon_1} < \sqrt{\omega/\rho}$ and $\sqrt{\varepsilon_1} \leq 1$. As the estimate is local, C does not depend on the size of $\mathscr{D}_\varepsilon$ [18, Theorem A.3]. Since $\|\bar{z}_\varepsilon\| \leq C$ by Lemma 2 and the $C^{3,\alpha}$ norm contains all derivatives up to order three, we obtain

$$\left\| \frac{\partial^{m+n} \bar{z}_\varepsilon}{\partial \nu^m \partial \eta^n} \right\|_{\bar{N}_\delta} \leq C,$$

for all non-negative integers m and n such that $1 \leq m+n \leq 3$. Since (ν_0, η_0) is chosen arbitrarily, this estimate extends globally across the domain $\bar{\mathscr{D}}_\varepsilon$. Reverting to the original spatial variables (x,y), the chain rule yields $\frac{\partial}{\partial x} = \frac{\partial \nu}{\partial x}\frac{\partial}{\partial \nu} = \varepsilon_1^{-1/2}\frac{\partial}{\partial \nu}$ and $\frac{\partial}{\partial y} = \frac{\partial \eta}{\partial y}\frac{\partial}{\partial \eta} = \varepsilon_1^{-1/2}\frac{\partial}{\partial \eta}$. Applying these differential operators m and n times respectively to the uniformly bounded transformed derivatives directly extracts the factor $(\varepsilon_1^{-1/2})^m(\varepsilon_1^{-1/2})^n = \varepsilon_1^{-(m+n)/2}$, providing the required estimate for this regime.

Case (ii): $\rho\varepsilon_2^2 \geq \omega\varepsilon_1$. For the convection-dominated regime, the domain is stretched using $\nu = \frac{\varepsilon_2}{\varepsilon_1}x$ and $\eta = \frac{\varepsilon_2}{\varepsilon_1}y$, which maps $\mathscr{D}$ to $\tilde{\mathscr{D}}_\varepsilon = (0, \varepsilon_2/\varepsilon_1)^2$ with boundary $\tilde{\mathscr{B}}_\varepsilon$. Expressing the system in terms of $\bar{z}_\varepsilon(\nu,\eta) = \bar{z}(x,y)$ and dividing by the positive scaling factor $\varepsilon_2^2/\varepsilon_1$, we obtain:

$$\left(\frac{\partial^2 \bar{z}_\varepsilon}{\partial \nu^2} + \frac{\partial^2 \bar{z}_\varepsilon}{\partial \eta^2}\right) + \mathbf{P}_\varepsilon(\nu,\eta)\frac{\partial \bar{z}_\varepsilon}{\partial \nu} - \frac{\varepsilon_1}{\varepsilon_2^2}\mathbf{Q}_\varepsilon(\nu,\eta)\bar{z}_\varepsilon(\nu,\eta) = \frac{\varepsilon_1}{\varepsilon_2^2}\bar{r}_\varepsilon(\nu,\eta).$$

In this regime, the condition $\rho\varepsilon_2^2 \geq \omega\varepsilon_1$ ensures that the transformed reaction coefficient and source term satisfy $\frac{\varepsilon_1}{\varepsilon_2^2} \leq \frac{\rho}{\omega} \leq C$. Therefore, the differential operator remains uniformly elliptic, with all coefficients bounded by constants independent of both perturbation parameters. The transformed problem is again subject to the homogeneous Dirichlet boundary conditions ($\bar{z}_\varepsilon = \bar{0}$ on $\tilde{\mathscr{B}}_\varepsilon$). Employing a localized neighborhood argument identical to that in Case (i), we apply the classical Schauder *a priori* estimates [16] over an arbitrary neighborhood $\tilde{\bar{N}}_\delta$ within $\tilde{\bar{\mathscr{D}}}_\varepsilon$. The coupling term is absorbed as in Case (i). The Hölder norms of the coefficients are again bounded, as $\varepsilon_1/\varepsilon_2 \leq (\rho/\omega)\,\varepsilon_2$. This yields the uniformly bounded derivative estimates

$$\left\| \frac{\partial^{m+n} \bar{z}_\varepsilon}{\partial \nu^m \partial \eta^n} \right\|_{\tilde{\bar{N}}_\delta} \leq C$$

for $1 \leq m+n \leq 3$. Reverting to the original spatial variables (x,y) via the chain rule yields $\frac{\partial}{\partial x} = \frac{\partial \nu}{\partial x}\frac{\partial}{\partial \nu} = \left(\frac{\varepsilon_2}{\varepsilon_1}\right)\frac{\partial}{\partial \nu}$ and $\frac{\partial}{\partial y} = \frac{\partial \eta}{\partial y}\frac{\partial}{\partial \eta} = \left(\frac{\varepsilon_2}{\varepsilon_1}\right)\frac{\partial}{\partial \eta}$. Applying these differential operators m and n times respectively extracts the exact scaling factor $\left(\frac{\varepsilon_2}{\varepsilon_1}\right)^{m+n} = \left(\frac{\varepsilon_1}{\varepsilon_2}\right)^{-(m+n)}$, yielding the desired estimate. □

2.1 Solution decomposition

In order to decompose the solution, we first identify the inflow, outflow and characteristic boundaries of problem (1). To this end, we multiply (1) by -1 and write it in the standard convection-diffusion form [18, 21], in which

Corrected Proof

the Laplacian has a negative coefficient,

$$-\varepsilon_1\Delta\bar{z}-\varepsilon_2\mathbf{P}(x,y)\frac{\partial\bar{z}}{\partial x}+\mathbf{Q}(x,y)\bar{z}=-\bar{r}(x,y),\quad (x,y)\in\mathscr{D}.$$

The convective velocity of the i-th equation is then the coefficient of its first-order term, $(-\varepsilon_2 p_i,0)^T$. Since $p_i\geq\rho>0$, its scalar product with the outward unit normal n is $-\varepsilon_2 p_i<0$ on $\mathscr{B}_3$, $\varepsilon_2 p_i>0$ on $\mathscr{B}_1$ and 0 on $\mathscr{B}_2\cup\mathscr{B}_4$. Hence $\mathscr{B}_3$ ($x=1$) is the inflow boundary, $\mathscr{B}_1$ ($x=0$) is the outflow boundary, and $\mathscr{B}_2$, $\mathscr{B}_4$ are characteristic boundaries. Setting $\varepsilon_1=0$ in (1) gives the reduced problem of the convection-dominated regime,

$$\varepsilon_2\mathbf{P}(x,y)\frac{\partial\bar{z}_0}{\partial x}-\mathbf{Q}(x,y)\bar{z}_0=\bar{r}(x,y),\quad (x,y)\in\mathscr{D}.$$

Its characteristics are the lines $y=$ const, traversed from $x=1$ to $x=0$. The data are therefore prescribed on the inflow boundary $\mathscr{B}_3$, and the condition on $\mathscr{B}_1$ is recovered by the outflow layer. Without the coupling term, each equation is the scalar problem $-\varepsilon\Delta u+\mu a u_x+bu=f$ of Hegarty and O'Riordan [12], with $\varepsilon=\varepsilon_1$, $a=p_i$, $b=q_{ii}$ and $\mu=-\varepsilon_2<0$. This is the case treated in their Remark 12. Below, we adapt their arguments to the system, with the roles of the inflow and outflow boundaries interchanged as in that remark.

Further, when two perturbation parameters are involved, the widths of the boundary layers depend on the ratio $\varepsilon_2^2/\varepsilon_1$. For the model problem (1), this gives rise to two distinct regimes, the reaction-dominated regime ($\rho\varepsilon_2^2<\omega\varepsilon_1$) and the convection-dominated regime ($\rho\varepsilon_2^2\geq\omega\varepsilon_1$). The regime determines the layers in the x-direction. In the reaction-dominated regime, the layers at $\mathscr{B}_1$ and $\mathscr{B}_3$ both have width $\mathscr{O}(\sqrt{\varepsilon_1})$. In the convection-dominated regime, a strong layer of width $\mathscr{O}(\varepsilon_1/\varepsilon_2)$ forms at the outflow boundary $\mathscr{B}_1$ and a weaker layer of width $\mathscr{O}(\varepsilon_2)$ forms at the inflow boundary $\mathscr{B}_3$. In the y-direction, characteristic layers of width $\mathscr{O}(\sqrt{\varepsilon_1})$ form along $\mathscr{B}_2$ and $\mathscr{B}_4$ in both regimes. Corner layers appear at the four vertices of $\mathscr{D}$, where the layers in the x- and y-directions meet.

Following this layer structure, we decompose the solution into a regular component and boundary and corner layer components. As in [20], some of these components are defined on rectangles slightly larger than $\mathscr{D}$. For a fixed $\delta>0$, let

$$\mathscr{D}^*=(-\delta,1+\delta)\times(-\delta,1+\delta),\qquad \mathscr{D}_R^*=(-\delta,1)\times(-\delta,1+\delta),$$
$$\mathscr{D}_L^*=(0,1)\times(-\delta,1+\delta),\quad \mathscr{D}_C^*=(-\delta,1+\delta)\times(0,1),\qquad \mathscr{D}_R^{**}=(-\delta,1)\times(0,1).$$

The regular component is constructed on $\mathscr{D}^*$, the inflow, outflow and characteristic layer components on $\mathscr{D}_R^*$, $\mathscr{D}_L^*$ and $\mathscr{D}_C^*$, respectively, and the inflow corner components on $\mathscr{D}_R^{**}$. The outflow corner components are defined on $\mathscr{D}$ itself. We denote by $\mathscr{B}^*$ the boundary of $\mathscr{D}^*$ and by $\mathscr{B}_3^*=\{1+\delta\}\times[-\delta,1+\delta]$ its right edge. We extend $\mathbf{P}$, $\mathbf{Q}$ and $\bar{r}$ smoothly to $\bar{\mathscr{D}}^*$ and denote the extensions by $\mathbf{P}^*$, $\mathbf{Q}^*$ and $\bar{r}^*$. These extensions are chosen to satisfy (2) and $q_{ii}-q_{ij}>2\omega p_i$ on $\bar{\mathscr{D}}^*$. Since all the rectangles above lie in $\mathscr{D}^*$, these extensions are used on each of them. Each corner of these rectangles is either a vertex of $\bar{\mathscr{D}}$ or lies outside $\bar{\mathscr{D}}$, so no compatibility conditions arise on $\bar{\mathscr{D}}$ other than those at its vertices. Near the corners outside $\bar{\mathscr{D}}$, we take $\mathbf{P}^*$ and $\mathbf{Q}^*$ constant and $\bar{r}^*=\bar{0}$. This does not change the problem on $\bar{\mathscr{D}}$. We write $\mathscr{L}^*_{\varepsilon_1,\varepsilon_2}$ for the operator obtained from $\mathscr{L}_{\varepsilon_1,\varepsilon_2}$ by replacing its coefficients with their extensions. Lemma 1 and the argument of Lemma 3 hold for $\mathscr{L}^*_{\varepsilon_1,\varepsilon_2}$ on each of these rectangles, with the same proofs.

The analysis of the components uses the following operators, all with the extended coefficients. Setting $\varepsilon_1=\varepsilon_2=0$ and $\varepsilon_1=0$ in $\mathscr{L}^*_{\varepsilon_1,\varepsilon_2}$ gives the reduced operators

$$\mathscr{L}_0^*\bar{w}=-\mathbf{Q}^*\bar{w},\qquad \mathscr{L}_{\varepsilon_2}^*\bar{w}=\varepsilon_2\mathbf{P}^*\frac{\partial\bar{w}}{\partial x}-\mathbf{Q}^*\bar{w},$$

which govern the regular component in the reaction-dominated and the convection-dominated regime, respectively. We now construct each component and derive its bounds, starting with the regular component.

Corrected Proof

Regular component. The regular component $\bar{u}$ satisfies

$$\mathscr{L}_{\varepsilon_1,\varepsilon_2}\bar{u} = \bar{r} \quad \text{in } \mathscr{D}. \tag{5}$$

Its values on $\mathscr{B}$ are not prescribed. Instead, $\bar{u}$ is the restriction to $\bar{\mathscr{D}}$ of a function $\bar{u}^*$ constructed on $\bar{\mathscr{D}}^*$ by an expansion based on the reduced problems, and this construction fixes them. By (2), $\mathbf{Q}^*$ is strictly diagonally dominant and hence invertible, so the algebraic problems below have unique smooth solutions.

In the reaction-dominated regime ($\rho\varepsilon_2^2 < \omega\varepsilon_1$), the reduced problems are algebraic, and we expand $\bar{u}^* = \bar{u}_0 + \sqrt{\varepsilon_1}\,\bar{u}_1 + \varepsilon_1\bar{u}_2$. The terms $\bar{u}_0$ and $\bar{u}_1$ are defined on $\bar{\mathscr{D}}^*$ by

$$\mathscr{L}_0^*\bar{u}_0 = \bar{r}^*, \qquad \mathscr{L}_0^*\bar{u}_1 = -\sqrt{\varepsilon_1}\,\Delta\bar{u}_0 - \frac{\varepsilon_2}{\sqrt{\varepsilon_1}}\mathbf{P}^*\frac{\partial\bar{u}_0}{\partial x},$$

and the remainder $\bar{u}_2$ solves

$$\mathscr{L}^*_{\varepsilon_1,\varepsilon_2}\bar{u}_2 = -\sqrt{\varepsilon_1}\,\Delta\bar{u}_1 - \frac{\varepsilon_2}{\sqrt{\varepsilon_1}}\mathbf{P}^*\frac{\partial\bar{u}_1}{\partial x} \ \text{ in } \mathscr{D}^*, \qquad \bar{u}_2 = \bar{0} \ \text{ on } \mathscr{B}^*.$$

Since $\varepsilon_2/\sqrt{\varepsilon_1} < \sqrt{\omega/\rho}$ in this regime, the right-hand side of the problem for $\bar{u}_1$ and its derivatives are bounded independently of the perturbation parameters. Hence $\left\|\frac{\partial^{m+n}\bar{u}_k}{\partial x^m\partial y^n}\right\|_{\mathscr{D}} \le C$ for $k = 0,1$. The remainder $\bar{u}_2$ solves an elliptic problem with zero boundary values and a bounded right-hand side. Hence the argument of Lemma 3 gives $\left\|\frac{\partial^{m+n}\bar{u}_2}{\partial x^m\partial y^n}\right\|_{\mathscr{D}} \le C\varepsilon_1^{-(m+n)/2}$. Substituting these bounds into the expansion of $\bar{u}^*$ gives

$$\left\|\frac{\partial^{m+n}\bar{u}}{\partial x^m\partial y^n}\right\|_{\mathscr{D}} \le C\left(1+\varepsilon_1^{\frac{2-(m+n)}{2}}\right).$$

In the convection-dominated regime ($\rho\varepsilon_2^2 \ge \omega\varepsilon_1$), the reduced operator is the first-order operator $\mathscr{L}^*_{\varepsilon_2}$. Since the flow is directed towards decreasing x, problems for $\mathscr{L}^*_{\varepsilon_2}$ are posed with data only on $\mathscr{B}_3^*$, the inflow part of $\mathscr{B}^*$. We expand $\bar{u}^* = \bar{u}_0^* + \varepsilon_1\bar{u}_1^* + \varepsilon_1^2\bar{u}_2^*$ and, as in the proof of [12, Lemma 1], write the first two terms as expansions in powers of ε_2,

$$\bar{u}_0^* = \sum_{i=0}^{4}\varepsilon_2^i\,\bar{s}_i, \qquad \bar{u}_1^* = \sum_{i=0}^{2}\varepsilon_2^i\,\bar{t}_i.$$

Here $\bar{s}_0,\dots,\bar{s}_3$ and $\bar{t}_0,\bar{t}_1$ solve algebraic problems on $\bar{\mathscr{D}}^*$, and $\bar{s}_4$, $\bar{t}_2$ solve first-order problems in $\mathscr{D}^*$ with zero data on $\mathscr{B}_3^*$. These problems are

$$\begin{aligned}
&\mathscr{L}_0^*\bar{s}_0 = \bar{r}^*, && \mathscr{L}_0^*\bar{s}_i = -\mathbf{P}^*\,\partial\bar{s}_{i-1}/\partial x \ \ (i=1,2,3), && \mathscr{L}^*_{\varepsilon_2}\bar{s}_4 = -\mathbf{P}^*\,\partial\bar{s}_3/\partial x,\\
&\mathscr{L}_0^*\bar{t}_0 = -\Delta\bar{u}_0^*, && \mathscr{L}_0^*\bar{t}_1 = -\mathbf{P}^*\,\partial\bar{t}_0/\partial x, && \mathscr{L}^*_{\varepsilon_2}\bar{t}_2 = -\mathbf{P}^*\,\partial\bar{t}_1/\partial x.
\end{aligned}$$

The remainder $\bar{u}_2^*$ solves $\mathscr{L}^*_{\varepsilon_1,\varepsilon_2}\bar{u}_2^* = -\Delta\bar{u}_1^*$ in $\mathscr{D}^*$, with $\bar{u}_2^* = \bar{0}$ on $\mathscr{B}^*$. A direct calculation shows that $\mathscr{L}^*_{\varepsilon_2}\bar{u}_0^* = \bar{r}^*$ and $\mathscr{L}^*_{\varepsilon_2}\bar{u}_1^* = -\Delta\bar{u}_0^*$, so that $\mathscr{L}^*_{\varepsilon_1,\varepsilon_2}\bar{u}^* = \bar{r}^*$ in $\mathscr{D}^*$. Since $\bar{s}_4 = \bar{0}$ on $\mathscr{B}_3^*$, the reduced solution $\bar{u}_0^*$ satisfies $\bar{u}_0^* = \bar{s}_0 + \varepsilon_2\bar{s}_1 + \varepsilon_2^2\bar{s}_2 + \varepsilon_2^3\bar{s}_3$ on $\mathscr{B}_3^*$, and no condition is imposed on the rest of $\mathscr{B}^*$.

As $\bar{s}_0,\dots,\bar{s}_3$ do not depend on the perturbation parameters, bounding $\bar{s}_4$ and $\bar{t}_2$ in the stretched variable x/ε_2 gives, for $0 \le m+n \le 3$,

$$\left\|\frac{\partial^{m+n}\bar{u}_0^*}{\partial x^m\partial y^n}\right\|_{\mathscr{D}^*} \le C, \qquad \left\|\frac{\partial^{m+n}\bar{u}_1^*}{\partial x^m\partial y^n}\right\|_{\mathscr{D}^*} \le C\left(1+\varepsilon_2^{2-m}\right).$$

In particular, $\Delta\bar{u}_1^*$ is bounded on $\mathscr{D}^*$. The remainder $\bar{u}_2^*$ therefore solves an elliptic problem with zero boundary values and a bounded right-hand side. Hence the argument of Lemma 3 gives $\left\|\frac{\partial^{m+n}\bar{u}_2^*}{\partial x^m\partial y^n}\right\|_{\mathscr{D}} \le C\left(\frac{\varepsilon_1}{\varepsilon_2}\right)^{-(m+n)}$. Because

Corrected Proof

$\varepsilon_1 \le (\rho/\omega)\varepsilon_2^2$, we have $\varepsilon_1 \varepsilon_2^{2-m} \le C$ for $m \le 3$. Substituting these bounds into the expansion of $\bar{u}^*$ gives

$$\left\| \frac{\partial^{m+n} \bar{u}}{\partial x^m \partial y^n} \right\|_{\bar{\mathscr{D}}} \le C \left(1 + \frac{\varepsilon_1^{2-(m+n)}}{\varepsilon_2^{-(m+n)}} \right).$$

Continuing the expansions in both regimes with further terms gives bounds on the derivatives of $\bar{u}$ up to order five, which imply the ones above. We take $\bar{u}^*$ to be given by these longer expansions, so that the traces of $\bar{u}^*$ used as data in the layer problems below are smooth enough.

Boundary layer components. The boundary layer components correct the boundary values of $\bar{u}$ edge by edge. These are the inflow layer $\bar{v}^R$ at $\mathscr{B}_3$, the outflow layer $\bar{v}^L$ at $\mathscr{B}_1$, and the characteristic layers $\bar{v}^B$ and $\bar{v}^T$ at $\mathscr{B}_2$ and $\mathscr{B}_4$. They are defined by

$$\begin{aligned}
&\mathscr{L}^*_{\varepsilon_1,\varepsilon_2} \bar{v}^k = \bar{0} \ \text{ in } \mathscr{D}_k^*,\ k \in \{L,R\}, \quad \mathscr{L}^*_{\varepsilon_1,\varepsilon_2} \bar{v}^k = \bar{0} \ \text{ in } \mathscr{D}_C^*,\ k \in \{B,T\},\\
&\bar{v}^R(1,y) = (\bar{z} - \bar{u}^*)(1,y),\ -\delta \le y \le 1+\delta, \quad \bar{v}^R = \bar{0} \text{ on the other sides of } \mathscr{D}_R^*,\\
&\bar{v}^L(0,y) = (\bar{z} - \bar{u}^* - \bar{v}^R)(0,y),\ -\delta \le y \le 1+\delta, \quad \bar{v}^L = \bar{0} \text{ on the other sides of } \mathscr{D}_L^*,\\
&\bar{v}^B(x,0) = (\bar{z} - \bar{u}^*)(x,0),\ -\delta \le x \le 1+\delta, \quad \bar{v}^B = \bar{0} \text{ on the other sides of } \mathscr{D}_C^*,\\
&\bar{v}^T(x,1) = (\bar{z} - \bar{u}^*)(x,1),\ -\delta \le x \le 1+\delta, \quad \bar{v}^T = \bar{0} \text{ on the other sides of } \mathscr{D}_C^*,
\end{aligned} \tag{6}$$

where $\bar{z}$ is extended smoothly outside $\bar{\mathscr{D}}$ so that these data vanish near the corners of the extended rectangles. Hence $\bar{u} + \bar{v}^R = \bar{z}$ on $\mathscr{B}_3$, $\bar{u} + \bar{v}^R + \bar{v}^L = \bar{z}$ on $\mathscr{B}_1$, and $\bar{u} + \bar{v}^B = \bar{z}$, $\bar{u} + \bar{v}^T = \bar{z}$ on $\mathscr{B}_2$ and $\mathscr{B}_4$, respectively. The traces that these components leave on the neighboring edges are removed by the corner layer components defined below.

The layer components are analyzed as in the scalar case [12, Section 2]. That analysis requires positive lower bounds on the convection and reaction coefficients and on their ratio, and smooth data that are compatible at the corners. For the system, the corresponding conditions are $p_i \ge \rho$ and $q_{ii} - q_{ij} \ge \gamma^2$ from (2), $(q_{ii} - q_{ij})/p_i > 2\omega$ from the choice of ω, and the smoothness and the corner condition $\bar{r} = \bar{0}$ of Section 1. In every problem below, the coupling enters only through the zero-order term $-\mathbf{Q}^*$. The argument of Lemma 1 therefore gives a comparison principle for each of these problems, and barrier functions with equal components lead to the factor $q_{ii} - q_{ij}$ in place of the scalar reaction coefficient. The derivative bounds follow from local estimates of the type used in the proof of Lemma 3. Let $\bar{v} = (v_1, v_2)^T$ denote any of the boundary or corner layer components, or a term in one of their expansions below. As in that proof, the estimates are applied to the i-th equation, with the coupling term $q_{ij} v_j$, $j \ne i$, moved to the right-hand side. The coupling term is then absorbed as in the proof of Lemma 3, also in the parabolic estimates used below, with $\|\bar{v}\|$ bounded by the comparison principle. Hence the constants depend only on the data and on ρ, γ, ω and δ.

Pointwise bounds: We use the decay rates

$$\lambda_1 = \begin{cases} \dfrac{\sqrt{\omega\rho}}{2\sqrt{\varepsilon_1}}, & \rho\varepsilon_2^2 < \omega\varepsilon_1, \\ \dfrac{\rho\varepsilon_2}{2\varepsilon_1}, & \rho\varepsilon_2^2 \ge \omega\varepsilon_1, \end{cases} \qquad \lambda_2 = \begin{cases} \dfrac{\sqrt{\omega\rho}}{2\sqrt{\varepsilon_1}}, & \rho\varepsilon_2^2 < \omega\varepsilon_1, \\ \dfrac{\omega}{2\varepsilon_2}, & \rho\varepsilon_2^2 \ge \omega\varepsilon_1, \end{cases}$$

for the layers at $x = 0$ and $x = 1$, respectively. They also determine the mesh transition points in Section 3. For example, consider the outflow layer and the barrier functions $\bar{\Psi}_L^{\pm}(x,y) = \bar{C} e^{-\lambda_1 x} \pm \bar{v}^L(x,y)$. Since $\bar{C}$ has equal components, the i-th component of $\mathscr{L}^*_{\varepsilon_1,\varepsilon_2}(\bar{C} e^{-\lambda_1 x})$ is $C\big(\varepsilon_1\lambda_1^2 - \varepsilon_2 p_i \lambda_1 - (q_{ii} - q_{ij})\big) e^{-\lambda_1 x} < 0$ in both regimes, because $p_i \ge \rho$ and $q_{ii} - q_{ij} > 2\omega p_i$. Hence $\mathscr{L}^*_{\varepsilon_1,\varepsilon_2} \bar{\Psi}_L^{\pm} \le \bar{0}$ in $\mathscr{D}_L^*$. Since $\bar{\Psi}_L^{\pm} \ge \bar{0}$ on the boundary of $\mathscr{D}_L^*$ for C large enough, Lemma 1 gives

$$|v_i^L(x,y)| \le C e^{-\lambda_1 x}, \qquad i = 1,2.$$

The bounds on the other components follow in the same way. For $\bar{v}^R$, we use $\bar{C} e^{-\lambda_2(1-x)}$ on $\mathscr{D}_R^*$, together with $\varepsilon_2/\sqrt{\varepsilon_1} < \sqrt{\omega/\rho}$ in the reaction-dominated regime and $\varepsilon_1/\varepsilon_2^2 \le \rho/\omega$ in the convection-dominated regime. For $\bar{v}^B$

Corrected Proof

and $\bar{v}^T$, we use $\bar{C}e^{-\gamma y/\sqrt{\varepsilon_1}}$ and $\bar{C}e^{-\gamma(1-y)/\sqrt{\varepsilon_1}}$ on $\mathscr{D}_C^*$, together with $q_{ii}-q_{ij}\geq\gamma^2$. This gives, for $i=1,2$,

$$|v_i^R(x,y)|\leq Ce^{-\lambda_2(1-x)},\qquad |v_i^B(x,y)|\leq Ce^{-\gamma y/\sqrt{\varepsilon_1}},\qquad |v_i^T(x,y)|\leq Ce^{-\gamma(1-y)/\sqrt{\varepsilon_1}}.$$

Derivative bounds: The local a priori estimates used in the proof of Lemma 3 are applied in the stretched variables $(x/\kappa, y/\kappa)$ and in their one-dimensional and parabolic analogues. Here $\kappa:=\varepsilon_1/(\varepsilon_2+\sqrt{\varepsilon_1})$ is of order $\sqrt{\varepsilon_1}$ in the reaction-dominated regime and of order $\varepsilon_1/\varepsilon_2$ in the convection-dominated regime. In these variables, after division by ε_1/κ^2, the coefficients are $(\varepsilon_2\kappa/\varepsilon_1)\mathbf{P}^*$ and $(\kappa^2/\varepsilon_1)\mathbf{Q}^*$. They are bounded, together with their Hölder norms, independently of ε_1 and ε_2 in both regimes, since $\varepsilon_2\kappa/\varepsilon_1<1$, $\kappa^2/\varepsilon_1\leq 1$ and $\kappa\leq 1$. For the outflow layer, applying these estimates to $\mathscr{L}^*_{\varepsilon_1,\varepsilon_2}\bar{v}^L=\bar{0}$ and, with the minimum principle, to the problem satisfied by $\partial_y\bar{v}^L$ gives

$$\left\|\frac{\partial^m\bar{v}^L}{\partial x^m}\right\|\leq\begin{cases}C\varepsilon_1^{-m/2}, & \rho\varepsilon_2^2<\omega\varepsilon_1,\\ C\left(\dfrac{\varepsilon_1}{\varepsilon_2}\right)^{-m}, & \rho\varepsilon_2^2\geq\omega\varepsilon_1,\end{cases}\qquad \left\|\frac{\partial^n\bar{v}^L}{\partial y^n}\right\|\leq\begin{cases}C\left(1+\varepsilon_1^{(1-n)/2}\right), & \rho\varepsilon_2^2<\omega\varepsilon_1,\\ C\left(1+\left(\dfrac{\varepsilon_1}{\varepsilon_2}\right)^{1-n}\right), & \rho\varepsilon_2^2\geq\omega\varepsilon_1.\end{cases}$$

The inflow layer $\bar{v}^R$ is treated in the same way in the reaction-dominated regime and satisfies the same bounds there. In the convection-dominated regime, $\bar{v}^R$ is a layer of width $\mathscr{O}(\varepsilon_2)$ at the inflow boundary, and it is expanded in powers of ε_1. For each fixed y, the leading term and the first correction solve two-point problems for $\varepsilon_1\partial_{xx}+\mathscr{L}^*_{\varepsilon_2}$ on $(-\delta,1)$, and the remainder solves an elliptic problem on $\mathscr{D}_R^*$. The two-point solutions are in turn expanded about solutions of first-order problems for $\mathscr{L}^*_{\varepsilon_2}$ with data on $x=1$, which vary on the scale ε_2. The remaining terms are bounded in the stretched variable $(1-x)/\kappa$ by one-dimensional and local estimates. This gives

$$\left\|\frac{\partial^m\bar{v}^R}{\partial x^m}\right\|\leq C\left(\varepsilon_2^{-m}+\varepsilon_1^{2-m}\varepsilon_2^{m-4}\right),\qquad \left\|\frac{\partial^n\bar{v}^R}{\partial y^n}\right\|\leq C\left(1+\varepsilon_2^{1-n}+\varepsilon_1^{2-n}\varepsilon_2^{n}\right).$$

These are the bounds of the inflow layer in the scalar case [12]. They remain valid for the system because every problem in this expansion is coupled only through $-\mathbf{Q}^*$. The comparison principle and the local estimates above therefore apply to the system. In the reaction-dominated regime, the characteristic layers $\bar{v}^k$, $k\in\{B,T\}$, are expanded in powers of $\sqrt{\varepsilon_1}$. The first two terms solve problems for the reaction-diffusion operator $\varepsilon_1\Delta-\mathbf{Q}^*$ on $\mathscr{D}_C^*$, and the remainder, which solves an elliptic problem there, is bounded by local estimates. In the convection-dominated regime, $\bar{v}^k$ is expanded in powers of ε_1. The leading terms solve problems for the parabolic operator $\mathscr{L}_p^*:=(\varepsilon_1\partial_{yy}-\mathbf{Q}^*)+\varepsilon_2\mathbf{P}^*\partial_x$, and the remainder solves an elliptic problem on $\mathscr{D}_C^*$. The first two parabolic terms are in turn expanded in powers of ε_2 about solutions of two-point problems for $\varepsilon_1\partial_{yy}-\mathbf{Q}^*$ on $(0,1)$, for each fixed x. The remaining terms are bounded by parabolic estimates in the stretched variables $(x/\varepsilon_2, y/\sqrt{\varepsilon_1})$ and by local estimates. In both regimes this gives

$$\left\|\frac{\partial^m\bar{v}^k}{\partial x^m}\right\|\leq C\left(1+\varepsilon_1^{2-m}\right),\qquad \left\|\frac{\partial^n\bar{v}^k}{\partial y^n}\right\|\leq C\varepsilon_1^{-n/2}.$$

Corner layer components. Finally, the corner layer components are defined by

$$\begin{aligned}
&\mathscr{L}^*_{\varepsilon_1,\varepsilon_2}\bar{v}^k=\bar{0}\ \text{ in }\mathscr{D}_R^{**},\ k\in\{BR,TR\},\qquad \mathscr{L}_{\varepsilon_1,\varepsilon_2}\bar{v}^k=\bar{0}\ \text{ in }\mathscr{D},\ k\in\{BL,TL\},\\
&\bar{v}^{BR}(x,0)=-\bar{v}^R(x,0),\ -\delta\leq x\leq 1,\quad \bar{v}^{BR}(1,y)=-\bar{v}^B(1,y),\quad \bar{v}^{BR}(-\delta,y)=\bar{v}^{BR}(x,1)=\bar{0},\\
&\bar{v}^{TR}(x,1)=-\bar{v}^R(x,1),\ -\delta\leq x\leq 1,\quad \bar{v}^{TR}(1,y)=-\bar{v}^T(1,y),\quad \bar{v}^{TR}(-\delta,y)=\bar{v}^{TR}(x,0)=\bar{0},\\
&\bar{v}^{BL}=-(\bar{v}^B+\bar{v}^{BR})\text{ on }\mathscr{B}_1,\quad \bar{v}^{BL}=-\bar{v}^L\text{ on }\mathscr{B}_2,\quad \bar{v}^{BL}=\bar{0}\text{ on }\mathscr{B}_3\cup\mathscr{B}_4,\\
&\bar{v}^{TL}=-(\bar{v}^T+\bar{v}^{TR})\text{ on }\mathscr{B}_1,\quad \bar{v}^{TL}=-\bar{v}^L\text{ on }\mathscr{B}_4,\quad \bar{v}^{TL}=\bar{0}\text{ on }\mathscr{B}_2\cup\mathscr{B}_3.
\end{aligned}\tag{7}$$

With these data, $\bar{u}+\sum_k\bar{v}^k=\bar{z}$ on $\mathscr{B}$ and $\mathscr{L}_{\varepsilon_1,\varepsilon_2}\left(\bar{u}+\sum_k\bar{v}^k\right)=\bar{r}$ in $\mathscr{D}$, so $\bar{z}=\bar{u}+\sum_k\bar{v}^k$ in $\bar{\mathscr{D}}$. The corner data are compatible at the vertices of $\bar{\mathscr{D}}$, so all components are smooth enough on $\bar{\mathscr{D}}$.

Corrected Proof

Pointwise bounds: These are obtained as for the boundary layer components, with product barrier functions such as $\bar{\Psi}^{\pm}_{BL}(x,y) = \bar{C}e^{-\lambda_1 x}e^{-\gamma y/(2\sqrt{\varepsilon_1})} \pm \bar{v}^{BL}(x,y)$. The rate in y is halved so that the factor in y adds at most $(q_{ii}-q_{ij})/4$ to the i-th component, and $\mathscr{L}^*_{\varepsilon_1,\varepsilon_2}\bar{\Psi}^{\pm}_{BL} \le \bar{0}$ still holds. Lemma 1 then gives

$$|v_i^{BL}(x,y)| \le Ce^{-\lambda_1 x}e^{-\gamma y/(2\sqrt{\varepsilon_1})}, \qquad i=1,2,$$

and the corresponding bounds at the other corners, which are listed in Theorem 1.

Derivative bounds: In the reaction-dominated regime, the argument of Lemma 3 gives $\|\partial^{m+n}\bar{v}^k/\partial x^m\partial y^n\| \le C\varepsilon_1^{-(m+n)/2}$ for all layer components. In the convection-dominated regime, the outflow corner components are treated as $\bar{v}^L$, by the local estimates in the variables $(x/\kappa, y/\kappa)$. Like $\bar{v}^R$, the inflow corner components are expanded in powers of ε_1 into two terms that solve problems for $\mathscr{L}^*_p$ on $\mathscr{D}^{**}_R$ and an elliptic remainder. At the corners $(0,0)$ and $(1,0)$, these arguments give

$$\left\|\frac{\partial^{m+n}\bar{v}^{BL}}{\partial x^m\partial y^n}\right\| \le C\left(\frac{\varepsilon_1}{\varepsilon_2}\right)^{-(m+n)}, \qquad \left\|\frac{\partial^{m+n}\bar{v}^{BR}}{\partial x^m\partial y^n}\right\| \le C\varepsilon_1^{-n/2}\left(\varepsilon_2^{-m}+\varepsilon_1^{2-m}\varepsilon_2^{m-4}\right),$$

together with the sharper bound $\|\partial^3\bar{v}^{BL}/\partial y^3\| \le C(\varepsilon_1/\varepsilon_2)^{-2}$, which follows, as for $\bar{v}^L$, from the problem satisfied by $\partial_y\bar{v}^{BL}$. Here, the bound for $\bar{v}^{BR}$ combines the scale ε_2 of $\bar{v}^R$ in x with the scale $\sqrt{\varepsilon_1}$ of $\bar{v}^B$ in y. These bounds also hold for the coupled corner problems, since the coupling enters only through the zero-order term. Further, the same bounds hold for $\bar{v}^{TL}$ and $\bar{v}^{TR}$, respectively.

The following theorem collects the decomposition and the bounds on its components, all restricted to $\bar{\mathscr{D}}$.

Theorem 1. *Let $\bar{z}(x,y)$ be the solution to the continuous system (1). Then, $\bar{z}$ admits a decomposition of the form:*

$$\bar{z} = \bar{u} + \bar{v}^B + \bar{v}^T + \bar{v}^L + \bar{v}^R + \bar{v}^{BL} + \bar{v}^{BR} + \bar{v}^{TL} + \bar{v}^{TR}, \tag{8}$$

where $\bar{u}$ represents the regular component and $\bar{v}^k$ for $k \in \{T,B,L,R,BL,BR,TL,TR\}$ denote the layer components. For $1 \le m+n \le 3$, the regular component satisfies:

$$\left\|\frac{\partial^{m+n}\bar{u}}{\partial x^m\partial y^n}\right\| \le \begin{cases} C\left(1+\varepsilon_1^{\frac{2-(m+n)}{2}}\right), & \rho\varepsilon_2^2 < \omega\varepsilon_1, \\ C\left(1+\dfrac{\varepsilon_1^{2-(m+n)}}{\varepsilon_2^{-(m+n)}}\right), & \rho\varepsilon_2^2 \ge \omega\varepsilon_1. \end{cases} \tag{9}$$

The pointwise bounds for the boundary and corner layer components are as follows, for $i=1,2$:

$$|v_i^B(x,y)| \le Ce^{-\frac{\gamma y}{\sqrt{\varepsilon_1}}}, \qquad |v_i^{BL}(x,y)| \le Ce^{-\lambda_1 x}e^{-\frac{\gamma y}{2\sqrt{\varepsilon_1}}},$$
$$|v_i^T(x,y)| \le Ce^{-\frac{\gamma(1-y)}{\sqrt{\varepsilon_1}}}, \qquad |v_i^{BR}(x,y)| \le Ce^{-\lambda_2(1-x)}e^{-\frac{\gamma y}{2\sqrt{\varepsilon_1}}},$$
$$|v_i^L(x,y)| \le Ce^{-\lambda_1 x}, \qquad |v_i^{TL}(x,y)| \le Ce^{-\lambda_1 x}e^{-\frac{\gamma(1-y)}{2\sqrt{\varepsilon_1}}},$$
$$|v_i^R(x,y)| \le Ce^{-\lambda_2(1-x)}, \qquad |v_i^{TR}(x,y)| \le Ce^{-\lambda_2(1-x)}e^{-\frac{\gamma(1-y)}{2\sqrt{\varepsilon_1}}}.$$

In addition, for $1 \le m,n \le 3$, we have

$$\left\|\frac{\partial^m\bar{v}^k}{\partial x^m}\right\| \le C\left(1+\varepsilon_1^{2-m}\right), \qquad \left\|\frac{\partial^n\bar{v}^k}{\partial y^n}\right\| \le C\varepsilon_1^{-n/2}, \quad k\in\{B,T\},$$

$$\left\|\frac{\partial^m\bar{v}^L}{\partial x^m}\right\| \le \begin{cases} C\varepsilon_1^{-m/2}, & \rho\varepsilon_2^2 < \omega\varepsilon_1, \\ C\left(\dfrac{\varepsilon_1}{\varepsilon_2}\right)^{-m}, & \rho\varepsilon_2^2 \ge \omega\varepsilon_1, \end{cases} \qquad \left\|\frac{\partial^n\bar{v}^L}{\partial y^n}\right\| \le \begin{cases} C\left(1+\varepsilon_1^{(1-n)/2}\right), & \rho\varepsilon_2^2 < \omega\varepsilon_1, \\ C\left(1+\left(\dfrac{\varepsilon_1}{\varepsilon_2}\right)^{1-n}\right), & \rho\varepsilon_2^2 \ge \omega\varepsilon_1. \end{cases}$$

Corrected Proof

$$\left\|\frac{\partial^m \bar{v}^R}{\partial x^m}\right\| \leq \begin{cases} C\varepsilon_1^{-m/2}, & \rho\varepsilon_2^2 < \omega\varepsilon_1, \\ C\left(\varepsilon_2^{-m} + \varepsilon_1^{2-m}\varepsilon_2^{m-4}\right), & \rho\varepsilon_2^2 \geq \omega\varepsilon_1, \end{cases} \quad \left\|\frac{\partial^n \bar{v}^R}{\partial y^n}\right\| \leq \begin{cases} C\left(1+\varepsilon_1^{(1-n)/2}\right), & \rho\varepsilon_2^2 < \omega\varepsilon_1, \\ C\left(1+\varepsilon_2^{1-n} + \varepsilon_1^{2-n}\varepsilon_2^{n}\right), & \rho\varepsilon_2^2 \geq \omega\varepsilon_1. \end{cases}$$

Moreover, for $1 \leq m+n \leq 3$, *when* $\rho\varepsilon_2^2 < \omega\varepsilon_1$ *and* $k \in \{T,B,L,R,BL,BR,TL,TR\}$,

$$\left\|\frac{\partial^{m+n} \bar{v}^k}{\partial x^m \partial y^n}\right\| \leq C\varepsilon_1^{-(m+n)/2}.$$

For $\rho\varepsilon_2^2 \geq \omega\varepsilon_1$, *the corner layer components satisfy*

$$\left\|\frac{\partial^{m+n} \bar{v}^k}{\partial x^m \partial y^n}\right\| \leq \begin{cases} C\left(\dfrac{\varepsilon_1}{\varepsilon_2}\right)^{-(m+n)}, & k \in \{BL,TL\}, \\ C\varepsilon_1^{-n/2}\left(\varepsilon_2^{-m} + \varepsilon_1^{2-m}\varepsilon_2^{m-4}\right), & k \in \{BR,TR\}, \end{cases}$$

and the sharper bound $\left\|\dfrac{\partial^3 \bar{v}^k}{\partial y^3}\right\| \leq C\left(\dfrac{\varepsilon_1}{\varepsilon_2}\right)^{-2}$ *holds for* $k \in \{BL,TL\}$.

3 Discretization of the problem

This section constructs a tailored piecewise-uniform Shishkin mesh for the spatial domain and develops a finite difference scheme for (1).

3.1 Mesh construction

The domain $\mathscr{D}$ is discretized into N subintervals (where $N \geq 4$ is assumed to be an integer multiple of four) using a Shishkin mesh, which is constructed by allocating equal resolution to both the layer and smooth regions of the solution. To separate these regions, the transition points are defined according to the width of the boundary layers in the two principal regimes, as described below.

In the x-direction, the layer behavior differs between the two regimes; therefore, the transition points are defined separately for each regime as follows:

$$\tau_{x_1} = \begin{cases} \min\left\{\frac{1}{4}, \frac{2\sqrt{\varepsilon_1}}{\sqrt{\rho\omega}}\ln N\right\}, & \rho\varepsilon_2^2 < \omega\varepsilon_1, \\ \min\left\{\frac{1}{4}, \frac{2\varepsilon_1}{\rho\varepsilon_2}\ln N\right\}, & \rho\varepsilon_2^2 \geq \omega\varepsilon_1, \end{cases} \quad \tau_{x_2} = \begin{cases} \min\left\{\frac{1}{4}, \frac{2\sqrt{\varepsilon_1}}{\sqrt{\rho\omega}}\ln N\right\}, & \rho\varepsilon_2^2 < \omega\varepsilon_1, \\ \min\left\{\frac{1}{4}, \frac{2\varepsilon_2}{\omega}\ln N\right\}, & \rho\varepsilon_2^2 \geq \omega\varepsilon_1. \end{cases}$$

In the y-direction, the layer behavior is the same in both regimes. Therefore, the transition point is defined as

$$\tau_y = \min\left\{\frac{1}{4}, \frac{2\sqrt{\varepsilon_1}}{\gamma}\ln N\right\}.$$

Because the transition parameters are restricted by the minimum with $1/4$, we have $\tau_{x_1} \leq 1/4$ and $\tau_{x_2} \leq 1/4$. This prevents the left and right fine-mesh regions from overlapping (since $\tau_{x_1} < 1 - \tau_{x_2}$).

Furthermore, these transition points correspond to the numerical layer widths. For small values of the parameters, they are formulated as $\tau_{x_i} = \lambda_i^{-1}\ln N$ for $i = 1,2$, where λ_i represent the respective continuous decay parameters in the x-direction (and similarly $\gamma/(2\sqrt{\varepsilon_1})$ in the y-direction). This guarantees that the layer components are fully captured within the fine mesh, as they decay to the level of the truncation error at the transition interfaces. For instance, evaluating the left boundary layer bound $\mathscr{O}(e^{-\lambda_1 x})$ at $x = \tau_{x_1}$ directly yields $e^{-\lambda_1\tau_{x_1}} = N^{-1}$. Analogous estimates hold for the remaining transition points, so the singular components are $\mathscr{O}(N^{-1})$ in the regular mesh regions.

Corrected Proof

Using these transition points, the layer and smooth regions in both directions can be distinguished according to their behavior in the two regimes. For the x-direction, the interval is decomposed as

$$[0,1] = [0,\tau_{x_1}] \cup [\tau_{x_1}, 1-\tau_{x_2}] \cup [1-\tau_{x_2}, 1].$$

Similarly, the y-interval is decomposed as

$$[0,1] = [0,\tau_y] \cup [\tau_y, 1-\tau_y] \cup [1-\tau_y, 1].$$

We allocate $N/4$ mesh intervals uniformly to each of the layer subintervals $[0,\tau_{x_1}], [1-\tau_{x_2},1], [0,\tau_y], [1-\tau_y,1]$, and $N/2$ mesh intervals to the corresponding smooth subintervals $[\tau_{x_1}, 1-\tau_{x_2}]$ and $[\tau_y, 1-\tau_y]$. Subsequently, the mesh points are given by

$$x_i = \begin{cases} ih_1, & \text{for } i = 0,\ldots,\frac{N}{4}, \\ \tau_{x_1} + \left(i-\frac{N}{4}\right)H, & \text{for } i = \frac{N}{4}+1,\ldots,\frac{3N}{4}, \\ (1-\tau_{x_2}) + \left(i-\frac{3N}{4}\right)h_2, & \text{for } i = \frac{3N}{4}+1,\ldots,N, \end{cases}$$

$$y_j = \begin{cases} jk_1, & \text{for } j = 0,\ldots,\frac{N}{4}, \\ \tau_y + (j-\frac{N}{4})K, & \text{for } j = \frac{N}{4}+1,\ldots,\frac{3N}{4}, \\ (1-\tau_y) + (j-\frac{3N}{4})k_2, & \text{for } j = \frac{3N}{4}+1,\ldots,N. \end{cases}$$

Here, the mesh distances between successive grid points, denoted by $h_i = x_i - x_{i-1}$ in x-space and $k_j = y_j - y_{j-1}$ in y-space, are given by

$$h_1 = \frac{4\tau_{x_1}}{N}, \quad H = \frac{2(1-\tau_{x_1}-\tau_{x_2})}{N}, \quad h_2 = \frac{4\tau_{x_2}}{N},$$
$$k_1 = \frac{4\tau_y}{N}, \quad K = \frac{2(1-2\tau_y)}{N}, \quad k_2 = \frac{4\tau_y}{N}.$$

With this discretization, we denote the discrete domain by $\mathscr{D}^{N,N}$ with boundary $\mathscr{B}^{N,N}$, and set $\bar{\mathscr{D}}^{N,N} = \mathscr{D}^{N,N} \cup \mathscr{B}^{N,N}$.

3.2 Finite difference scheme

On the discrete domain $\mathscr{D}^{N,N}$, we will construct an upwind scheme for the problem (1) using the following discrete operators:

$$\delta_x^2 \bar{W}_{i,j} = \frac{1}{\bar{h}_i}\left(D_x^+ \bar{W}_{i,j} - D_x^- \bar{W}_{i,j}\right), \; \delta_y^2 \bar{W}_{i,j} = \frac{1}{\bar{k}_j}\left(D_y^+ \bar{W}_{i,j} - D_y^- \bar{W}_{i,j}\right),$$
$$D_x^- \bar{W}_{i,j} = \frac{\bar{W}_{i,j} - \bar{W}_{i-1,j}}{h_i}, \qquad D_x^+ \bar{W}_{i,j} = \frac{\bar{W}_{i+1,j} - \bar{W}_{i,j}}{h_{i+1}},$$
$$D_y^- \bar{W}_{i,j} = \frac{\bar{W}_{i,j} - \bar{W}_{i,j-1}}{k_j}, \qquad D_y^+ \bar{W}_{i,j} = \frac{\bar{W}_{i,j+1} - \bar{W}_{i,j}}{k_{j+1}},$$
$$\bar{h}_i = \frac{h_i + h_{i+1}}{2}, \qquad \bar{k}_j = \frac{k_j + k_{j+1}}{2}.$$

Next, based on the sign pattern of the differential operator in (1) and the positivity of the convection coefficients ($p_1, p_2 \geq \rho > 0$), it is appropriate to use the forward upwind difference D_x^+ for the convective term (the flow is directed towards $x = 0$; see Subsection 2.1). This choice ensures the discrete system maintains the M-matrix property, which in turn guarantees numerical stability and aligns with the characteristic flow. Thus, using the above difference operators, we define the finite difference scheme for the problem (1) by

$$\begin{cases} \mathscr{L}^{N,N}_{\varepsilon_1,\varepsilon_2} \bar{Z}_{i,j} \equiv \varepsilon_1(\delta_x^2 + \delta_y^2)\bar{Z}_{i,j} + \varepsilon_2 \mathbf{P}_{i,j} D_x^+ \bar{Z}_{i,j} - \mathbf{Q}_{i,j}\bar{Z}_{i,j} = \bar{r}_{i,j}, \text{ in } \mathscr{D}^{N,N}, \\ \bar{Z}_{i,j} = \bar{0}, \text{ on } \mathscr{B}^{N,N}. \end{cases} \tag{10}$$

Corrected Proof

Lemma 4 (Discrete minimum principle)**.** *Let $\mathscr{L}^{N,N}_{\varepsilon_1,\varepsilon_2}$ denote the discrete operator (10). Suppose that a mesh function $\bar{\Phi}(x_i,y_j)$ satisfies $\bar{\Phi}(x_i,y_j)\geq \bar{0}$ on $\mathscr{B}^{N,N}$, and $\mathscr{L}^{N,N}_{\varepsilon_1,\varepsilon_2}\bar{\Phi}(x_i,y_j)\leq \bar{0}$ in $\mathscr{D}^{N,N}$. Then, $\bar{\Phi}(x_i,y_j)\geq \bar{0}$ for all $(x_i,y_j)\in\bar{\mathscr{D}}^{N,N}$.*

Lemma 5 (Discrete stability result)**.** *The discrete solution $\bar{Z}_{i,j}$ corresponding to (10) satisfies*

$$\|\bar{Z}\|_{\bar{\mathscr{D}}^{N,N}}\leq \max_{(x_i,y_j)\in\mathscr{B}^{N,N}}\left\{\|\bar{Z}(x_i,y_j)\|\right\}+\frac{1}{\gamma^2}\|\bar{r}\|_{\bar{\mathscr{D}}^{N,N}}.$$

The proofs of these two lemmas follow those of Lemmas 1 and 2, with differences in place of derivatives. This is possible because, with the upwind difference D_x^+ and $q_{ij}>0$, the matrix of $\mathscr{L}^{N,N}_{\varepsilon_1,\varepsilon_2}$ has negative diagonal entries and nonnegative off-diagonal entries.

4 Error analysis

This section presents a detailed error analysis of the proposed scheme (10). To obtain a sharp estimate, the error is analyzed separately for each component of the solution. For this purpose, we introduce discrete solution components analogous to those in the continuous setting. Accordingly, the discrete solution is decomposed into a regular component and several layer components as follows:

$$\bar{Z}=\bar{U}+\bar{V}^B+\bar{V}^T+\bar{V}^L+\bar{V}^R+\bar{V}^{BL}+\bar{V}^{BR}+\bar{V}^{TL}+\bar{V}^{TR}. \tag{11}$$

Here, $\bar{U}$ denotes the discrete regular component, while $\bar{V}^k$ represent the discrete layer components. The components $\bar{V}^k$ with indices $k\in\{B,T,L,R\}$ correspond to the boundary layer components, and $k\in\{BL,BR,TL,TR\}$ denote the corner layer components. These components are obtained as solutions of the following discrete problems:

$$\begin{aligned}\mathscr{L}^{N,N}_{\varepsilon_1,\varepsilon_2}\bar{U}(x_i,y_j)&=\bar{r}(x_i,y_j), && (x_i,y_j)\in\mathscr{D}^{N,N},\\ \bar{U}(x_i,y_j)&=\bar{u}(x_i,y_j), && (x_i,y_j)\in\mathscr{B}^{N,N},\end{aligned} \tag{12}$$

$$\begin{aligned}\mathscr{L}^{N,N}_{\varepsilon_1,\varepsilon_2}\bar{V}^k(x_i,y_j)&=\bar{0}, && (x_i,y_j)\in\mathscr{D}^{N,N},\\ \bar{V}^k(x_i,y_j)&=\bar{v}^k(x_i,y_j), && (x_i,y_j)\in\mathscr{B}^{N,N},\end{aligned} \tag{13}$$

for $k\in\{B,T,L,R,BL,BR,TL,TR\}$. All error estimates below rest on the following truncation error bound, obtained by Taylor expansion: for a sufficiently smooth function $\bar{v}$ and $(x_i,y_j)\in\mathscr{D}^{N,N}$,

$$\left|\left(\mathscr{L}^{N,N}_{\varepsilon_1,\varepsilon_2}-\mathscr{L}_{\varepsilon_1,\varepsilon_2}\right)\bar{v}(x_i,y_j)\right|\leq C\left(\varepsilon_1(h_i+h_{i+1})\left\|\frac{\partial^3\bar{v}}{\partial x^3}\right\|+\varepsilon_1(k_j+k_{j+1})\left\|\frac{\partial^3\bar{v}}{\partial y^3}\right\|+\varepsilon_2 h_{i+1}\left\|\frac{\partial^2\bar{v}}{\partial x^2}\right\|\right).$$

In each lemma, this bound is combined with the derivative bounds of Theorem 1 and the mesh sizes $h_1=4\tau_{x_1}/N$, $h_2=4\tau_{x_2}/N$, $k_1=k_2=4\tau_y/N$ and $H,K\leq 2N^{-1}$ of Subsection 3.1. The regime condition used to control each parameter-dependent factor is stated where it is used. Throughout this section, the constants C depend only on the data and on ρ, γ, ω and δ, so they are independent of N, ε_1 and ε_2. We now discuss the error estimate for the regular component $\bar{U}$.

Lemma 6. *Let $\bar{U}$ and $\bar{u}$ be the solutions of the discrete problem (12) and the continuous problem (5), respectively. Then, for each $(x_i,y_j)\in\bar{\mathscr{D}}^{N,N}$,*

$$|\bar{U}(x_i,y_j)-\bar{u}(x_i,y_j)|\leq CN^{-1}. \tag{14}$$

Proof. The truncation error for the regular component is bounded by:

$$|\mathscr{L}^{N,N}_{\varepsilon_1,\varepsilon_2}(\bar{U}-\bar{u})(x_i,y_j)|\leq CN^{-1}\left(\varepsilon_1\left\|\frac{\partial^3\bar{u}}{\partial x^3}\right\|+\varepsilon_1\left\|\frac{\partial^3\bar{u}}{\partial y^3}\right\|+\varepsilon_2\left\|\frac{\partial^2\bar{u}}{\partial x^2}\right\|\right).$$

Corrected Proof

Substituting the derivative bounds from Theorem 1, we evaluate this for both parameter regimes.
Case (i): $\rho\varepsilon_2^2 < \omega\varepsilon_1$. Substituting the corresponding bounds yields:

$$|\mathscr{L}^{N,N}_{\varepsilon_1,\varepsilon_2}(\bar{U}-\bar{u})| \le CN^{-1}\left(\varepsilon_1(\varepsilon_1^{-1/2})+\varepsilon_1(\varepsilon_1^{-1/2})+\varepsilon_2(1)\right) \le CN^{-1}.$$

Case (ii): $\rho\varepsilon_2^2 \ge \omega\varepsilon_1$. Substituting the corresponding bounds yields:

$$|\mathscr{L}^{N,N}_{\varepsilon_1,\varepsilon_2}(\bar{U}-\bar{u})| \le CN^{-1}\left(\varepsilon_1\left(1+\frac{\varepsilon_2^3}{\varepsilon_1}\right)+\varepsilon_1\left(1+\frac{\varepsilon_2^3}{\varepsilon_1}\right)+\varepsilon_2(1+\varepsilon_2^2)\right) \le CN^{-1}.$$

Finally, applying Lemma 5 to these uniformly bounded truncation errors gives

$$|\bar{U}(x_i,y_j)-\bar{u}(x_i,y_j)| \le CN^{-1}, \tag{15}$$

for all $(x_i,y_j) \in \bar{\mathscr{D}}^{N,N}$. □

To obtain parameter-uniform error estimates for the singular components, we construct discrete barrier functions that capture the exponential decay of the continuous layer functions. Based on the characteristic decay rates established in Theorem 1, we define the following discrete barrier functions for the boundary layers:

$$\zeta_{\bar{V}^B;j} = \begin{cases} \prod_{m=1}^{j}(1+k_m\gamma/(2\sqrt{\varepsilon_1}))^{-1}, & j \ne 0, \\ 1, & j=0, \end{cases} \qquad \zeta_{\bar{V}^T;j} = \begin{cases} \prod_{m=j+1}^{N}(1+k_m\gamma/(2\sqrt{\varepsilon_1}))^{-1}, & j \ne N, \\ 1, & j=N, \end{cases}$$

$$\zeta_{\bar{V}^L;i} = \begin{cases} \prod_{m=1}^{i}(1+h_m\lambda_1)^{-1}, & i \ne 0, \\ 1, & i=0, \end{cases} \qquad \zeta_{\bar{V}^R;i} = \begin{cases} \prod_{m=i+1}^{N}(1+h_m\lambda_2)^{-1}, & i \ne N, \\ 1, & i=N. \end{cases}$$

Note that, for every j, we have

$$e^{(-\gamma y_j/\sqrt{\varepsilon_1})} \le e^{(-\gamma y_j/(2\sqrt{\varepsilon_1}))} = \prod_{m=1}^{j} e^{(-\gamma k_m/(2\sqrt{\varepsilon_1}))} \le \zeta_{\bar{V}^B;j},$$

and for $\tau_y < 1/4$ and $N/4 \le j \le N$, we also have

$$\zeta_{\bar{V}^B;j} \le \zeta_{\bar{V}^B;N/4} = \left(1+4N^{-1}\ln N\right)^{-N/4} \le CN^{-1}. \tag{16}$$

Moreover, regarding $\zeta_{\bar{V}^B;j}$ as a vector with two equal components, $q_{ii}-q_{ij} \ge \gamma^2$ gives

$$\mathscr{L}^{N,N}_{\varepsilon_1,\varepsilon_2}\zeta_{\bar{V}^B;j} \le -\frac{\gamma^2}{2}\zeta_{\bar{V}^B;j} \quad \text{in } \mathscr{D}^{N,N}. \tag{17}$$

By symmetry, $\zeta_{\bar{V}^T;j}$ satisfies the same bounds. For $\zeta = \zeta_{\bar{V}^L;i}$ and $\zeta = \zeta_{\bar{V}^R;i}$, the same computation with $q_{ii}-q_{ij} > 2\omega p_i$ in place of $q_{ii}-q_{ij} \ge \gamma^2$, together with the regime conditions for $\zeta_{\bar{V}^R;i}$, gives $\mathscr{L}^{N,N}_{\varepsilon_1,\varepsilon_2}\zeta \le -\omega\rho\,\zeta$ in both regimes. Since $\tau_{x_1} = \lambda_1^{-1}\ln N$ and $\tau_{x_2} = \lambda_2^{-1}\ln N$ when they are less than $1/4$, the bound (16) also holds for $\zeta_{\bar{V}^L;i}$ at $i = N/4$ and for $\zeta_{\bar{V}^R;i}$ at $i = 3N/4$. For the subsequent analysis, we focus on the case $\tau_{x_1} < 1/4$, $\tau_{x_2} < 1/4$ and $\tau_y < 1/4$; this allows us to examine the solution behavior in the most computationally challenging scenario, where the boundary layers are sharp and require the specific clustering of the Shishkin mesh. In cases where the transition points are $\tau_{x_1} = \tau_{x_2} = \tau_y = 1/4$, the mesh becomes uniform, and the result remains valid by noting that the parameters satisfy $\varepsilon_1^{-1/2} \le C\ln N$, $\varepsilon_2/\varepsilon_1 \le C\ln N$ or $\varepsilon_2^{-1} \le C\ln N$, so the estimates remain parameter-uniform.

Corrected Proof

Lemma 7. *Let $\bar{V}^k$ and $\bar{v}^k$ denote the solutions of the discrete problem (13) (for $k = B,T$) and the continuous problem (6), respectively. Then, for (x_i,y_j) in $\bar{\mathscr{D}}^{N,N}$, we have*

$$|\bar{V}^k(x_i,y_j) - \bar{v}^k(x_i,y_j)| \le CN^{-1}\ln N. \tag{18}$$

Proof. As the localized behavior of the top and bottom characteristic layers depends only on the parabolic scaling associated with ε_1, the resulting error bound is independent of the relation between the two parameters. Consequently, the same analysis applies to both parameter regimes ($\rho\varepsilon_2^2 < \omega\varepsilon_1$ and $\rho\varepsilon_2^2 \ge \omega\varepsilon_1$). We now begin the proof for the component $\bar{V}^B$.

From the definition of the discrete singular component and the continuous pointwise bounds presented in Theorem 1, it holds on the boundary $\mathscr{B}^{N,N}$ that

$$|\bar{V}^B(x_i,y_j)| = |\bar{v}^B(x_i,y_j)| \le Ce^{-\frac{\gamma_{y_j}}{\sqrt{\varepsilon_1}}} \le C\zeta_{\bar{V}^B;j}. \tag{19}$$

To exploit the mesh anisotropy, we partition the domain and define the fine mesh region in the y-direction corresponding to the layer width by $\mathscr{D}_B^{N,N} = \{(x_i,y_j) \mid 0 < i < N,\ 0 < j < N/4\}$.

First, consider the coarse mesh region far from the layer, defined by $(x_i,y_j) \in \bar{\mathscr{D}}^{N,N} \setminus \mathscr{D}_B^{N,N}$, where $j \ge N/4$. In this region, the continuous layer component has decayed significantly. Utilizing the triangle inequality along with the boundary tracking property from (19), which extends to $\bar{\mathscr{D}}^{N,N}$ by (17) and Lemma 4, and the discrete barrier function bounds, we obtain

$$|\bar{V}^B(x_i,y_j) - \bar{v}^B(x_i,y_j)| \le |\bar{V}^B(x_i,y_j)| + |\bar{v}^B(x_i,y_j)| \le C\zeta_{\bar{V}^B;N/4} \le CN^{-1}. \tag{20}$$

Next, we examine the points in the finer region $\mathscr{D}_B^{N,N}$, where the step size in the y-direction is $k_j = 4\tau_y/N$. Applying Taylor series expansion for the discrete operator, the local truncation error is governed by

$$|\mathscr{L}^{N,N}_{\varepsilon_1,\varepsilon_2}(\bar{V}^B - \bar{v}^B)(x_i,y_j)| \le CN^{-1}\left(\varepsilon_1\left\|\frac{\partial^3\bar{v}^B}{\partial x^3}\right\| + \varepsilon_1\tau_y\left\|\frac{\partial^3\bar{v}^B}{\partial y^3}\right\| + \varepsilon_2\left\|\frac{\partial^2\bar{v}^B}{\partial x^2}\right\|\right).$$

Substituting the derivative estimates from Theorem 1 into the truncation error expression and simplifying algebraically (noting that $\tau_y = \mathscr{O}(\sqrt{\varepsilon_1}\ln N)$) yields:

$$\begin{aligned}|\mathscr{L}^{N,N}_{\varepsilon_1,\varepsilon_2}(\bar{V}^B - \bar{v}^B)| &\le CN^{-1}\left(\varepsilon_1(\varepsilon_1^{-1}) + \varepsilon_1\tau_y(\varepsilon_1^{-3/2}) + \varepsilon_2(1)\right)\\ &\le CN^{-1}(1 + \ln N + \varepsilon_2) \le CN^{-1}\ln N.\end{aligned} \tag{21}$$

Then, using the barrier function $CN^{-1}\ln N$ and invoking the discrete minimum principle (Lemma 4) on $\mathscr{D}_B^{N,N}$, with (21) and the boundary values given by (20), we obtain $|\bar{V}^B - \bar{v}^B| \le CN^{-1}\ln N$ in $\mathscr{D}_B^{N,N}$. Together with (20), this gives the global error as

$$|\bar{V}^B(x_i,y_j) - \bar{v}^B(x_i,y_j)| \le CN^{-1}\ln N, \quad \forall (x_i,y_j) \in \bar{\mathscr{D}}^{N,N}. \tag{22}$$

For $\bar{V}^T$, the same argument applies with $\zeta_{\bar{V}^T;j}$ and the fine region $\{(x_i,y_j) \mid 0 < i < N,\ 3N/4 < j < N\}$, since $\bar{v}^T$ satisfies the same bounds as $\bar{v}^B$ in Theorem 1. This completes the proof. □

Lemma 8. *Let $\bar{V}^k$ and $\bar{v}^k$ be the solutions of the discrete problem (13) (for $k \in \{L,R\}$) and the continuous problem (6), respectively. Then, for (x_i,y_j) in $\bar{\mathscr{D}}^{N,N}$, we have the estimate*

$$|\bar{V}^L(x_i,y_j) - \bar{v}^L(x_i,y_j)| \le \begin{cases} CN^{-1}\ln N, & \rho\varepsilon_2^2 < \omega\varepsilon_1,\\ CN^{-1}(\ln N)^2, & \rho\varepsilon_2^2 \ge \omega\varepsilon_1,\end{cases}$$

$$|\bar{V}^R(x_i,y_j) - \bar{v}^R(x_i,y_j)| \le CN^{-1}\ln N.$$

Corrected Proof

Proof. For the left and right boundary layers, the localized behavior is highly sensitive to the ratio of the two parameters. Therefore, the analysis is carried out separately for the two parameter regimes. We first treat the left layer component $\bar{V}^L$, and the right layer component $\bar{V}^R$ is treated at the end of the proof. The variation of these components is confined to the layer regions, and the barrier functions built from λ_1 and λ_2 control them on the boundary and outside these regions. Thus, from the definition of the layer component (13) (for $k = L$) and using Theorem 1, for the points $(x_i, y_j) \in \mathscr{B}^{N,N}$ we obtain

$$|\bar{V}^L(x_i,y_j)| = |\bar{v}^L(x_i,y_j)| \le Ce^{-\lambda_1 x_i} \le C\zeta_{\bar{V}^L;i}. \tag{23}$$

We define the layer region corresponding to $\bar{v}^L$ by $\mathscr{D}_L^{N,N} = \{(x_i,y_j) \mid 0 < j < N,\ 0 < i < N/4\}$. Then for the points that are far from this layer region, that is for $(x_i,y_j) \in \mathscr{D}^{N,N} \setminus \mathscr{D}_L^{N,N}$, from (23), which extends to $\bar{\mathscr{D}}^{N,N}$ by the inequality $\mathscr{L}^{N,N}_{\varepsilon_1,\varepsilon_2}\zeta_{\bar{V}^L;i} \le -\omega\rho\,\zeta_{\bar{V}^L;i}$ and Lemma 4, and the bounds on the function $\zeta_{\bar{V}^L;i}$ we have

$$|\bar{V}^L(x_i,y_j) - \bar{v}^L(x_i,y_j)| \le |\bar{V}^L(x_i,y_j)| + |\bar{v}^L(x_i,y_j)| \le C\zeta_{\bar{V}^L;N/4} \le CN^{-1}. \tag{24}$$

For mesh points in the fine region, the two parameter regimes are treated separately by combining Taylor's expansion with the estimates from Theorem 1.

Case (i): $\rho\varepsilon_2^2 < \omega\varepsilon_1$. For points in the finer region $\mathscr{D}_L^{N,N}$, substituting the mesh step size $\tau_{x_1} = \mathscr{O}(\sqrt{\varepsilon_1}\ln N)$ and the derivative estimates from Theorem 1 into the truncation error yields

$$\begin{aligned}
|\mathscr{L}^{N,N}_{\varepsilon_1,\varepsilon_2}(\bar{V}^L - \bar{v}^L)| &\le CN^{-1}\left(\varepsilon_1\tau_{x_1}\left\|\frac{\partial^3\bar{v}^L}{\partial x^3}\right\| + \varepsilon_1\left\|\frac{\partial^3\bar{v}^L}{\partial y^3}\right\| + \varepsilon_2\tau_{x_1}\left\|\frac{\partial^2\bar{v}^L}{\partial x^2}\right\|\right)\\
&\le CN^{-1}\left(\varepsilon_1(\sqrt{\varepsilon_1}\ln N)(\varepsilon_1^{-3/2}) + \varepsilon_1(\varepsilon_1^{-1}) + \varepsilon_2(\sqrt{\varepsilon_1}\ln N)(\varepsilon_1^{-1})\right)\\
&\le CN^{-1}\left(\ln N + 1 + \frac{\varepsilon_2}{\sqrt{\varepsilon_1}}\ln N\right).
\end{aligned}$$

Applying the regime condition $\rho\varepsilon_2^2 < \omega\varepsilon_1$ guarantees that the intermediate factor satisfies $\frac{\varepsilon_2}{\sqrt{\varepsilon_1}} < \sqrt{\frac{\omega}{\rho}} \le C$, which removes the parameter dependence and gives

$$|\mathscr{L}^{N,N}_{\varepsilon_1,\varepsilon_2}(\bar{V}^L - \bar{v}^L)| \le CN^{-1}\ln N.$$

Then, using the barrier function $CN^{-1}\ln N$ and Lemma 4 on $\mathscr{D}_L^{N,N}$, with the boundary values given by (24), for $(x_i,y_j) \in \mathscr{D}_L^{N,N}$ we get the estimate

$$|\bar{V}^L(x_i,y_j) - \bar{v}^L(x_i,y_j)| \le CN^{-1}\ln N. \tag{25}$$

Case (ii): $\rho\varepsilon_2^2 \ge \omega\varepsilon_1$. For points in the finer region $\mathscr{D}_L^{N,N}$, using $\tau_{x_1} = \mathscr{O}\left(\frac{\varepsilon_1}{\varepsilon_2}\ln N\right)$ and the corresponding anisotropic derivative bounds from Theorem 1 for the convection-dominated regime, we obtain

$$\begin{aligned}
|\mathscr{L}^{N,N}_{\varepsilon_1,\varepsilon_2}(\bar{V}^L - \bar{v}^L)| &\le CN^{-1}\left(\varepsilon_1\tau_{x_1}\left\|\frac{\partial^3\bar{v}^L}{\partial x^3}\right\| + \varepsilon_1\left\|\frac{\partial^3\bar{v}^L}{\partial y^3}\right\| + \varepsilon_2\tau_{x_1}\left\|\frac{\partial^2\bar{v}^L}{\partial x^2}\right\|\right)\\
&\le CN^{-1}\left(\varepsilon_1\left(\frac{\varepsilon_1}{\varepsilon_2}\ln N\right)\left(\frac{\varepsilon_2^3}{\varepsilon_1^3}\right) + \varepsilon_1\left(\frac{\varepsilon_2^2}{\varepsilon_1^2}\right) + \varepsilon_2\left(\frac{\varepsilon_1}{\varepsilon_2}\ln N\right)\left(\frac{\varepsilon_2^2}{\varepsilon_1^2}\right)\right)\\
&\le C\left(\frac{\varepsilon_2^2}{\varepsilon_1}\right)N^{-1}\ln N.
\end{aligned}$$

Because $\rho\varepsilon_2^2 \ge \omega\varepsilon_1$, the factor $\frac{\varepsilon_2^2}{\varepsilon_1}$ cannot be bounded by a constant. To control this factor, we define the discrete barrier function $\bar{\Phi}_L^{\pm}(x_i,y_j) = \bar{\xi}(x_i,y_j) \pm (\bar{V}^L(x_i,y_j) - \bar{v}^L(x_i,y_j))$, where $\bar{\xi}(x_i,y_j) = \bar{C}\frac{\varepsilon_2}{\varepsilon_1}N^{-1}\ln N(\tau_{x_1} - x_i) + \bar{C}N^{-1}$.

Corrected Proof

Applying the discrete operator to $\bar{\xi}$ (and noting that the second-order difference operators evaluate to zero since $\bar{\xi}$ is linear in x_i and constant in y_j) yields $\mathscr{L}^{N,N}_{\varepsilon_1,\varepsilon_2}\bar{\xi}(x_i,y_j) = \varepsilon_2 \mathbf{P}_{i,j} D_x^+ \bar{\xi} - \mathbf{Q}_{i,j}\bar{\xi} \le -\bar{C}\rho\left(\frac{\varepsilon_2^2}{\varepsilon_1}\right) N^{-1}\ln N$. By choosing C sufficiently large, we ensure $\mathscr{L}^{N,N}_{\varepsilon_1,\varepsilon_2}\bar{\Phi}_L^{\pm} \le \bar{0}$. This C depends only on the constants in the truncation error bound above and in (24), so it is independent of N, ε_1 and ε_2. Furthermore, $\bar{\Phi}_L^{\pm} \ge \bar{0}$ on the boundary of $\mathscr{D}_L^{N,N}$, since the error vanishes on $\mathscr{B}^{N,N}$ and is at most CN^{-1} at $i = N/4$ by (24), which is the value of $\bar{\xi}$ at $x_i = \tau_{x_1}$. Thus, the discrete minimum principle (Lemma 4) on $\mathscr{D}_L^{N,N}$ implies $\bar{\Phi}_L^{\pm} \ge \bar{0}$, and consequently $|\bar{V}^L - \bar{v}^L| \le \bar{\xi}(x_i,y_j)$ in $\mathscr{D}_L^{N,N}$. Evaluating this bound at its maximum ($x_i = 0$) and substituting the transition point $\tau_{x_1} = \frac{2\varepsilon_1}{\rho\varepsilon_2}\ln N$ removes the perturbation parameters:

$$|\bar{V}^L(x_i,y_j) - \bar{v}^L(x_i,y_j)| \le \bar{\xi}(0,y_j) = C\frac{\varepsilon_2}{\varepsilon_1}N^{-1}\ln N\left(\frac{2\varepsilon_1}{\rho\varepsilon_2}\ln N\right) + CN^{-1} \le CN^{-1}(\ln N)^2, \tag{26}$$

for all $(x_i,y_j) \in \mathscr{D}_L^{N,N}$. Now, combining the coarse-region estimate (24) with the corresponding fine-region estimates (25) and (26), we obtain the estimates stated in the lemma.

We now treat the right layer component $\bar{V}^R$. Let $\mathscr{D}_R^{N,N}$ denote the set of mesh points with $3N/4 < i < N$ and $0 < j < N$. Outside $\mathscr{D}_R^{N,N}$ the bound CN^{-1} follows from $\zeta_{\bar{V}^R;i}$ as in (24). In $\mathscr{D}_R^{N,N}$, where $h_i = 4\tau_{x_2}/N$, the case $\rho\varepsilon_2^2 < \omega\varepsilon_1$ is identical to Case (i), since then $\tau_{x_2} = \tau_{x_1}$ and $\bar{v}^R$ satisfies the same bounds as $\bar{v}^L$ in Theorem 1. If $\rho\varepsilon_2^2 \ge \omega\varepsilon_1$, then $\tau_{x_2} = \frac{2\varepsilon_2}{\omega}\ln N$ and Theorem 1 give

$$\begin{aligned}
|\mathscr{L}^{N,N}_{\varepsilon_1,\varepsilon_2}(\bar{V}^R - \bar{v}^R)| &\le CN^{-1}\left(\varepsilon_1\tau_{x_2}\left\|\frac{\partial^3\bar{v}^R}{\partial x^3}\right\| + \varepsilon_1\left\|\frac{\partial^3\bar{v}^R}{\partial y^3}\right\| + \varepsilon_2\tau_{x_2}\left\|\frac{\partial^2\bar{v}^R}{\partial x^2}\right\|\right)\\
&\le CN^{-1}\left(\varepsilon_1\varepsilon_2\ln N\left(\varepsilon_2^{-3} + \varepsilon_1^{-1}\varepsilon_2^{-1}\right) + \varepsilon_1\left(1 + \varepsilon_2^{-2} + \varepsilon_2^3\varepsilon_1^{-1}\right)\right)\\
&\quad + CN^{-1}\varepsilon_2^2\ln N\,\varepsilon_2^{-2} \le CN^{-1}\ln N,
\end{aligned}$$

where the regime condition is used in the form $\varepsilon_1\varepsilon_2^{-2} \le \rho/\omega$. No factor $\varepsilon_2^2\varepsilon_1^{-1}$ appears, because the inflow layer has width $\mathscr{O}(\varepsilon_2)$, and Lemma 4 with a constant barrier gives $|\bar{V}^R - \bar{v}^R| \le CN^{-1}\ln N$ in $\mathscr{D}_R^{N,N}$ in both regimes. □

Lemma 9. *Let $\bar{V}^k$ and $\bar{v}^k$, $k \in \{BL, BR, TL, TR\}$, represent the solutions of the discrete and continuous problems (13) and (7), respectively. Then, for $(x_i,y_j) \in \bar{\mathscr{D}}^{N,N}$, the error satisfies:*

$$|\bar{V}^k(x_i,y_j) - \bar{v}^k(x_i,y_j)| \le \begin{cases} CN^{-1}\ln N, & \rho\varepsilon_2^2 < \omega\varepsilon_1,\\ CN^{-1}(\ln N)^2, & \rho\varepsilon_2^2 \ge \omega\varepsilon_1, \end{cases} \qquad \text{for } k \in \{BL, TL\},$$

$$|\bar{V}^k(x_i,y_j) - \bar{v}^k(x_i,y_j)| \le CN^{-1}\ln N, \qquad \text{for } k \in \{BR, TR\}.$$

Proof. As in (19) and (23), the pointwise bound of Theorem 1 gives

$$|\bar{V}^{BL}(x_i,y_j)| \le C\min\{\zeta_{\bar{V}^B;j}, \zeta_{\bar{V}^L;i}\},$$

for $(x_i,y_j) \in \mathscr{B}^{N,N}$. By (17), the inequality $\mathscr{L}^{N,N}_{\varepsilon_1,\varepsilon_2}\zeta_{\bar{V}^L;i} \le -\omega\rho\,\zeta_{\bar{V}^L;i}$ and Lemma 4, this bound also holds on $\bar{\mathscr{D}}^{N,N}$. Then from the bounds on the barrier functions $\zeta_{\bar{V}^B;j}$ and $\zeta_{\bar{V}^L;i}$, we get, for $i \ge N/4$ or $j \ge N/4$,

$$|\bar{V}^{BL}(x_i,y_j) - \bar{v}^{BL}(x_i,y_j)| \le CN^{-1}. \tag{27}$$

For the points in the finer region $\mathscr{D}_{BL}^{N,N} = \{(x_i,y_j) \mid 0 < i,j < N/4\}$, we evaluate the local truncation error by incorporating the transverse step size bounded by $k_j \le C\tau_y N^{-1}$. Using the truncation error bound stated at the beginning of this section, we address the two parameter regimes using Theorem 1.

Corrected Proof

Case (i): $\rho\varepsilon_2^2 < \omega\varepsilon_1$. For $(x_i,y_j) \in \mathscr{D}_{BL}^{N,N}$, substituting the mesh step sizes $\tau_{x_1}, \tau_y = \mathscr{O}(\sqrt{\varepsilon_1}\ln N)$ and the derivative estimates from Theorem 1 into the truncation error yields

$$\begin{aligned}|\mathscr{L}_{\varepsilon_1,\varepsilon_2}^{N,N}(\bar{V}^{BL}-\bar{v}^{BL})| &\le CN^{-1}\left(\varepsilon_1\tau_{x_1}\left\|\frac{\partial^3\bar{v}^{BL}}{\partial x^3}\right\| + \varepsilon_1\tau_y\left\|\frac{\partial^3\bar{v}^{BL}}{\partial y^3}\right\| + \varepsilon_2\tau_{x_1}\left\|\frac{\partial^2\bar{v}^{BL}}{\partial x^2}\right\|\right)\\ &\le CN^{-1}\left(\varepsilon_1(\sqrt{\varepsilon_1}\ln N)(\varepsilon_1^{-3/2}) + \varepsilon_1(\sqrt{\varepsilon_1}\ln N)(\varepsilon_1^{-3/2}) + \varepsilon_2(\sqrt{\varepsilon_1}\ln N)(\varepsilon_1^{-1})\right)\\ &\le CN^{-1}\ln N\left(1+1+\frac{\varepsilon_2}{\sqrt{\varepsilon_1}}\right).\end{aligned}$$

Applying the regime condition $\rho\varepsilon_2^2 < \omega\varepsilon_1$ guarantees that the intermediate factor satisfies $\frac{\varepsilon_2}{\sqrt{\varepsilon_1}} < \sqrt{\frac{\omega}{\rho}} \le C$ and gives

$$|\mathscr{L}_{\varepsilon_1,\varepsilon_2}^{N,N}(\bar{V}^{BL}-\bar{v}^{BL})| \le CN^{-1}\ln N.$$

Then, using the barrier function $CN^{-1}\ln N$ and Lemma 4 on $\mathscr{D}_{BL}^{N,N}$, with the boundary values given by (27), for $(x_i,y_j) \in \mathscr{D}_{BL}^{N,N}$ we obtain

$$|\bar{V}^{BL}(x_i,y_j) - \bar{v}^{BL}(x_i,y_j)| \le CN^{-1}\ln N. \tag{28}$$

Case (ii): $\rho\varepsilon_2^2 \ge \omega\varepsilon_1$. For $(x_i,y_j) \in \mathscr{D}_{BL}^{N,N}$, substituting the mesh step sizes $\tau_{x_1} = \mathscr{O}\left(\frac{\varepsilon_1}{\varepsilon_2}\ln N\right)$, $\tau_y = \mathscr{O}(\sqrt{\varepsilon_1}\ln N)$, and the corresponding anisotropic derivative bounds from Theorem 1 yields

$$\begin{aligned}|\mathscr{L}_{\varepsilon_1,\varepsilon_2}^{N,N}(\bar{V}^{BL}-\bar{v}^{BL})| &\le CN^{-1}\left(\varepsilon_1\tau_{x_1}\left\|\frac{\partial^3\bar{v}^{BL}}{\partial x^3}\right\| + \varepsilon_1\tau_y\left\|\frac{\partial^3\bar{v}^{BL}}{\partial y^3}\right\| + \varepsilon_2\tau_{x_1}\left\|\frac{\partial^2\bar{v}^{BL}}{\partial x^2}\right\|\right)\\ &\le CN^{-1}\left(\varepsilon_1\left(\frac{\varepsilon_1}{\varepsilon_2}\ln N\right)\left(\frac{\varepsilon_2^3}{\varepsilon_1^3}\right) + \varepsilon_1(\sqrt{\varepsilon_1}\ln N)\left(\frac{\varepsilon_2^2}{\varepsilon_1^2}\right) + \varepsilon_2\left(\frac{\varepsilon_1}{\varepsilon_2}\ln N\right)\left(\frac{\varepsilon_2^2}{\varepsilon_1^2}\right)\right)\\ &\le C\left(\frac{\varepsilon_2^2}{\varepsilon_1}\right)N^{-1}\ln N + CN^{-1}\ln N.\end{aligned}$$

Because $\rho\varepsilon_2^2 \ge \omega\varepsilon_1$, the factor $\frac{\varepsilon_2^2}{\varepsilon_1}$ cannot be bounded by a constant. To control this, we reuse the barrier function $\bar{\xi}(x_i,y_j)$ introduced in the previous lemma. As established, $\mathscr{L}_{\varepsilon_1,\varepsilon_2}^{N,N}\bar{\xi} \le -\bar{C}\rho\left(\frac{\varepsilon_2^2}{\varepsilon_1}\right)N^{-1}\ln N$, which dominates the truncation error bound displayed above. It also dominates the last term of that bound, since $\varepsilon_2^2/\varepsilon_1 \ge \omega/\rho$ in this regime. On the boundary of $\mathscr{D}_{BL}^{N,N}$, the error vanishes for $i=0$ or $j=0$ and is at most $CN^{-1} \le \bar{\xi}$ for $i = N/4$ or $j = N/4$ by (27), because $\bar{\xi} \ge \bar{C}N^{-1}$ in $\mathscr{D}_{BL}^{N,N}$. Applying the discrete minimum principle on $\mathscr{D}_{BL}^{N,N}$ using $\bar{\Phi}_{BL}^{\pm} = \bar{\xi} \pm (\bar{V}^{BL} - \bar{v}^{BL})$ ensures $|\bar{V}^{BL}(x_i,y_j) - \bar{v}^{BL}(x_i,y_j)| \le \bar{\xi}(x_i,y_j)$. As in Lemma 8, substituting the transition point τ_{x_1} reduces this bound to $\mathscr{O}(N^{-1}(\ln N)^2)$, independently of the perturbation parameters, which gives:

$$|\bar{V}^{BL}(x_i,y_j) - \bar{v}^{BL}(x_i,y_j)| \le CN^{-1}(\ln N)^2, \quad (x_i,y_j) \in \mathscr{D}_{BL}^{N,N}. \tag{29}$$

Combining the coarse region bound (27) with (28) and (29) completes the proof for the bottom-left corner layer component.

For $\bar{V}^{TL}$, Cases (i) and (ii) apply with $\zeta_{\bar{V}^T;j}$ in place of $\zeta_{\bar{V}^B;j}$ and the fine region $\{(x_i,y_j)\,|\,0<i<N/4,\ 3N/4<j<N\}$, since $\bar{v}^{TL}$ satisfies the same bounds as $\bar{v}^{BL}$ in Theorem 1. This gives the same estimate as for $\bar{V}^{BL}$. In contrast, the bottom-right and top-right corner layers ($\bar{V}^{BR}$ and $\bar{V}^{TR}$) are associated with the inflow boundary. For these, the bound outside the fine corner regions follows as above with $\zeta_{\bar{V}^R;i}$ in place of $\zeta_{\bar{V}^L;i}$, and inside them the case $\rho\varepsilon_2^2 < \omega\varepsilon_1$ is as in Case (i), since all corner components satisfy the same bounds in this regime. For $\rho\varepsilon_2^2 \ge \omega\varepsilon_1$, we have $\tau_{x_2} = \frac{2\varepsilon_2}{\omega}\ln N$, and Theorem 1 gives, in the fine corner region of $\bar{V}^{BR}$,

$$|\mathscr{L}_{\varepsilon_1,\varepsilon_2}^{N,N}(\bar{V}^{BR}-\bar{v}^{BR})| \le CN^{-1}\left(\varepsilon_1\tau_{x_2}\left\|\frac{\partial^3\bar{v}^{BR}}{\partial x^3}\right\| + \varepsilon_1\tau_y\left\|\frac{\partial^3\bar{v}^{BR}}{\partial y^3}\right\| + \varepsilon_2\tau_{x_2}\left\|\frac{\partial^2\bar{v}^{BR}}{\partial x^2}\right\|\right)$$

Corrected Proof

$$\leq CN^{-1}\ln N\left(\varepsilon_1\varepsilon_2\left(\varepsilon_2^{-3}+\varepsilon_1^{-1}\varepsilon_2^{-1}\right)+\varepsilon_1\sqrt{\varepsilon_1}\,\varepsilon_1^{-3/2}\left(1+\varepsilon_1^2\varepsilon_2^{-4}\right)+\varepsilon_2^2\,\varepsilon_2^{-2}\right)$$
$$\leq CN^{-1}\ln N\left(1+\varepsilon_1\varepsilon_2^{-2}+\varepsilon_1^2\varepsilon_2^{-4}\right)\leq CN^{-1}\ln N,$$

where the regime condition is used in the form $\varepsilon_1\varepsilon_2^{-2}\leq\rho/\omega$. Unlike $\bar{V}^{BL}$, no factor $\varepsilon_2^2/\varepsilon_1$ appears, since the inflow layer has width $\mathscr{O}(\varepsilon_2)$. Then, using the barrier function $CN^{-1}\ln N$ and Lemma 4 on the fine corner region, with the boundary values given by the bound outside it, we obtain the uniform estimate $CN^{-1}\ln N$. The same argument applies to $\bar{V}^{TR}$, since $\bar{v}^{TR}$ satisfies the same bounds as $\bar{v}^{BR}$ in Theorem 1. This completes the proof. □

Finally, we establish the main parameter-uniform convergence result for the proposed numerical scheme.

Theorem 2. *Let $\bar{z}(x_i,y_j)$ denote the continuous solution to the system (1), and let $\bar{Z}(x_i,y_j)$ be the approximation obtained from the difference scheme (10) on $\bar{\mathscr{D}}^{N,N}$. Then, there exists a constant C, independent of N, ε_1, and ε_2, such that the global error satisfies*

$$|\bar{Z}(x_i,y_j)-\bar{z}(x_i,y_j)|\leq\begin{cases}CN^{-1}\ln N, & \text{if } \rho\varepsilon_2^2<\omega\varepsilon_1,\\ CN^{-1}(\ln N)^2, & \text{if } \rho\varepsilon_2^2\geq\omega\varepsilon_1,\end{cases}\quad (x_i,y_j)\in\bar{\mathscr{D}}^{N,N}. \tag{30}$$

Proof. By the triangle inequality and the solution decompositions (8) and (11), the global nodal error is bounded by the sum of the errors associated with the regular, boundary layer, and corner layer components. Therefore, the required estimate follows immediately from Lemmas 6, 7, 8, and 9. □

Remark 1. *Although Theorem 2 establishes a theoretical parameter-uniform error bound of $\mathscr{O}(N^{-1}\ln N)$ for the reaction-dominated regime ($\rho\varepsilon_2^2<\omega\varepsilon_1$), the scheme exhibits a higher empirical convergence rate when ε_2 is sufficiently small. As $\varepsilon_2\to 0$, the continuous problem asymptotically reduces to a pure two-dimensional singularly perturbed reaction-diffusion system. In this limit, the truncation error of the first-order upwind approximation of the convection term, which carries the factor ε_2, becomes negligible, and the error comes mainly from the second-order central difference approximation of the diffusion term. Consequently, the numerical experiments exhibit an empirical convergence rate approaching second order when ε_2 is sufficiently small. We note that this is an empirical observation for restricted parameter spaces and is not part of the parameter-uniform estimate proved in Theorem 2. This behavior is discussed further in the numerical experiments section.*

5 Numerical results and discussion

In this section, we provide numerical evidence consistent with the theoretical convergence estimates of the proposed numerical scheme through two computational experiments. All computations are performed in MATLAB R2023b, utilizing sparse matrix data structures to optimize memory allocation and computational efficiency.

Since the exact analytical solutions for the model problems are unavailable, we estimate the maximum pointwise errors using the double-mesh principle [8]. For a given mesh resolution N and specific perturbation parameters ε_1 and ε_2, the double-mesh error is computed as

$$E^{N,N}_{\varepsilon_1,\varepsilon_2}=\max_{0\leq i,j\leq N}\left|\bar{Z}^{2N,2N}(x_{2i},y_{2j})-\bar{Z}^{N,N}(x_i,y_j)\right|,$$

where $\bar{Z}^{2N,2N}$ and $\bar{Z}^{N,N}$ represent the numerical solutions obtained on the fine mesh $\mathscr{D}^{2N,2N}$ and the coarse mesh $\mathscr{D}^{N,N}$, respectively. From this, the computed maximum pointwise error over the parameter values considered is

$$E^{N,N}=\max_{\varepsilon_1,\varepsilon_2}E^{N,N}_{\varepsilon_1,\varepsilon_2}.$$

Finally, the corresponding computed order of convergence is determined by:

$$Q^{N,N}=\log_2\left(\frac{E^{N,N}}{E^{2N,2N}}\right).$$

Corrected Proof

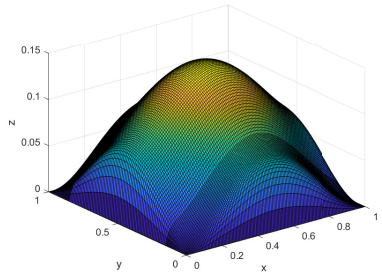

(a) Z_1 with $\varepsilon_1 = 2^{-12}$, $\varepsilon_2 = 2^{-9}$

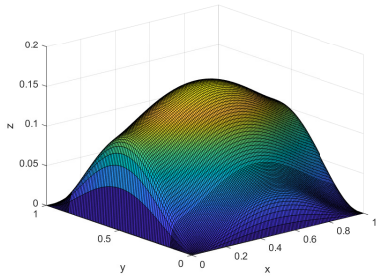

(b) Z_2 with $\varepsilon_1 = 2^{-12}$, $\varepsilon_2 = 2^{-9}$

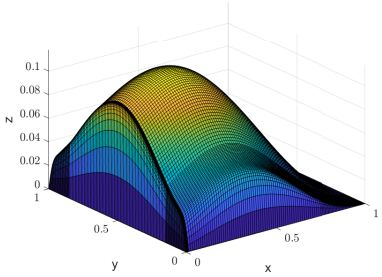

(c) Z_1 with $\varepsilon_1 = 2^{-12}$, $\varepsilon_2 = 2^{-3}$

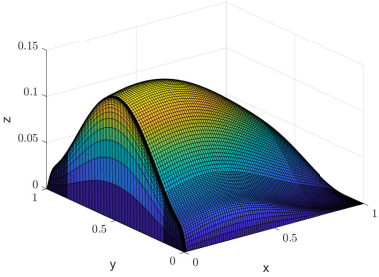

(d) Z_2 with $\varepsilon_1 = 2^{-12}$, $\varepsilon_2 = 2^{-3}$

Figure 1: Surface plots of the numerical solution for Example 1 with $N = 128$: (a), (b) the reaction-dominated regime with $\varepsilon_1 = 2^{-12}$, $\varepsilon_2 = 2^{-9}$; (c), (d) the convection-dominated regime with $\varepsilon_1 = 2^{-12}$, $\varepsilon_2 = 2^{-3}$

These double-mesh values are estimates of the error, and the results below provide numerical evidence consistent with the bounds proved in Section 4. Applying these metrics, we now present and analyze the computational results for the test problems.

Example 1. In problem (1), let $\mathbf{P}(x,y) = \mathrm{diag}(3,2)$, $\mathbf{Q}(x,y) = \begin{pmatrix} 3 & -2 \\ -2 & 3 \end{pmatrix}$, and $\bar{r}(x,y) = (-2x^2(1-x)^2, -3y^2(1-y)^2)^T$.

To examine the influence of the two parameter regimes on the computed solution, Figures 1 and 2 present the corresponding surface and contour plots for Example 1. The upper row shows the reaction-dominated case ($\rho\varepsilon_2^2 < \omega\varepsilon_1$), while the lower row corresponds to the convection-dominated case ($\rho\varepsilon_2^2 \geq \omega\varepsilon_1$). The numerical solutions capture the analytical layer structure discussed earlier. A comparison of the contour plots indicates that the boundary layers in the y-direction exhibit essentially the same behavior in both regimes, suggesting that they are unaffected by the ratio of the perturbation parameters. The principal differences are observed in the x-direction. In the reaction-dominated regime, layers of width $\mathscr{O}(\sqrt{\varepsilon_1})$ appear along all four boundaries. However, when the convection term becomes dominant, the layer profile in the x-direction changes and becomes strongly anisotropic.

Tables 1 and 2 present the maximum pointwise errors and convergence rates for the components Z_1 and Z_2 of Example 1, respectively, computed with a fixed $\varepsilon_2 = 2^{-6}$ and varying $\varepsilon_1 = 2^0, 2^{-3}, \ldots, 2^{-30}$ across mesh resolutions $N = 16, 32, \ldots, 512$. As observed in the data, for relatively large values of ε_1 (up to $\varepsilon_1 = 2^{-9}$), the convergence order is close to one (0.91–1.03 at $N = 512$). However, as ε_1 decreases further ($\varepsilon_1 \leq 2^{-12}$), the computed rate $Q^{N,N}$ reaches 0.714 for Z_1 and 0.742 for Z_2, which is consistent with the theoretical bound $\mathscr{O}(N^{-1}(\ln N)^2)$.

Furthermore, to illustrate Remark 1, Tables 3 and 4 display the error metrics for a fixed $\varepsilon_1 = 2^{-18}$ alongside a progressively varying convection parameter $\varepsilon_2 = 2^0, 2^{-3}, \ldots, 2^{-30}$. These tables show that as $\varepsilon_2 \to 0$, the convergence rate accelerates, reaching 1.653 for Z_1 and 1.619 for Z_2 at $N = 512$. These results provide numerical

Corrected Proof

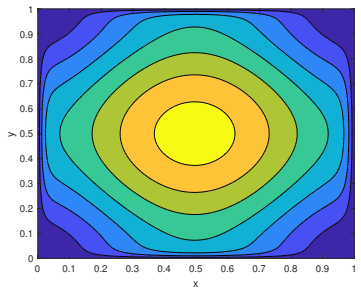

(a) Z_1 with $\varepsilon_1 = 2^{-12}$, $\varepsilon_2 = 2^{-9}$

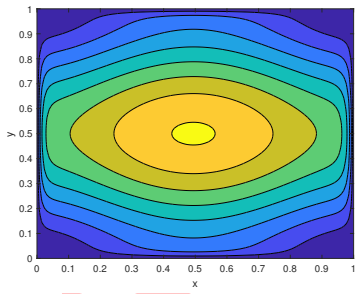

(b) Z_2 with $\varepsilon_1 = 2^{-12}$, $\varepsilon_2 = 2^{-9}$

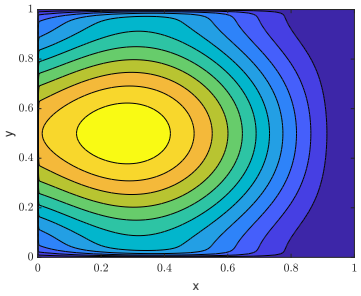

(c) Z_1 with $\varepsilon_1 = 2^{-12}$, $\varepsilon_2 = 2^{-3}$

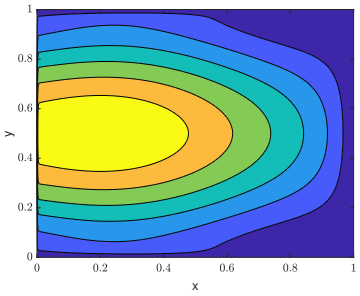

(d) Z_2 with $\varepsilon_1 = 2^{-12}$, $\varepsilon_2 = 2^{-3}$

Figure 2: Contour plots of the numerical solution for Example 1 with $N = 128$: (a), (b) the reaction-dominated regime with $\varepsilon_1 = 2^{-12}$, $\varepsilon_2 = 2^{-9}$; (c), (d) the convection-dominated regime with $\varepsilon_1 = 2^{-12}$, $\varepsilon_2 = 2^{-3}$

evidence consistent with Remark 1. When ε_2 is small, the convection term has little effect, the system behaves like a reaction-diffusion problem, and the computed rates empirically approach second order.

Example 2. For this example, choose $\mathbf{P}(x,y) = \mathrm{diag}(2+x, 1+x+y)$, $\mathbf{Q}(x,y) = \begin{pmatrix} 4+xy & -(2-xy) \\ -(1+x^2y) & 3+xy^2 \end{pmatrix}$ and $\bar{r}(x,y) = (-\sin(\pi xy), -\cos(\pi xy/2))^T$.

To examine the effect of a different set of coefficient functions, including source data that do not vanish at the corners, we consider Example 2, and the corresponding surface and contour plots are presented in Figures 3 and 4. The upper row shows the reaction-dominated regime ($\rho\varepsilon_2^2 < \omega\varepsilon_1$), whereas the lower row corresponds to the convection-dominated regime ($\rho\varepsilon_2^2 \geq \omega\varepsilon_1$). The numerical solutions display the same qualitative features observed in Example 1, suggesting that the proposed scheme resolves the layer structure satisfactorily despite the change in the convection coefficients. The contour plots further indicate that the principal differences between the two regimes arise in the x-direction, with increasingly anisotropic boundary layers in the convection-dominated regime, while the layer behavior in the transverse direction remains nearly unchanged, in agreement with the theoretical analysis.

The convergence behavior is further examined using the log–log plots of the maximum pointwise error shown in Figure 5 for Example 2. The plots are generated for different values of ε_1, while keeping $\varepsilon_2 = 2^{-3}$ fixed. For $\varepsilon_1 \in \{2^0, 2^{-3}\}$, the computed errors follow the expected $\mathcal{O}(N^{-1}\ln N)$ convergence trend. As ε_1 decreases to 2^{-24} and 2^{-27}, the error curves approach the theoretical $\mathcal{O}(N^{-1}(\ln N)^2)$ rate. The corresponding maximum pointwise errors are listed in Tables 5 and 6. The tabulated results show a steady reduction in the error as the mesh is refined, with the computed orders settling between 1.009 and 1.052 at $N = 512$ in the reaction-dominated regime, and the computed rate $Q^{N,N}$ reaching 0.698 for Z_1 and 0.695 for Z_2 in the convection-dominated regime.

To further illustrate the importance of the layer-adapted mesh, we compare the performance of the proposed

Table 1: Maximum pointwise error and convergence rate for Z_1 in Example 1 with fixed $\varepsilon_2 = 2^{-6}$

ε_1	$N=16$	$N=32$	$N=64$	$N=128$	$N=256$	$N=512$
Reaction-dominated regime ($\rho\varepsilon_2^2 < \omega\varepsilon_1$)						
2^0	4.129e-06	1.294e-06	4.821e-07	2.642e-07	1.452e-07	7.590e-08
Order	–	1.674	1.424	0.868	0.863	0.936
2^{-3}	9.028e-05	4.500e-05	2.268e-05	1.138e-05	5.698e-06	2.851e-06
Order	–	1.004	0.989	0.995	0.998	0.999
2^{-6}	7.375e-04	3.439e-04	1.638e-04	7.985e-05	3.941e-05	1.958e-05
Order	–	1.101	1.071	1.036	1.019	1.010
Convection-dominated regime ($\rho\varepsilon_2^2 \geq \omega\varepsilon_1$)						
2^{-9}	3.570e-03	2.375e-03	1.384e-03	7.557e-04	3.962e-04	2.031e-04
Order	–	0.588	0.779	0.873	0.932	0.964
2^{-12}	5.576e-03	5.206e-03	3.889e-03	2.748e-03	1.771e-03	1.076e-03
Order	–	0.099	0.421	0.501	0.634	0.719
2^{-15}	6.354e-03	5.836e-03	4.297e-03	3.068e-03	1.977e-03	1.205e-03
Order	–	0.123	0.442	0.486	0.634	0.715
2^{-18}	6.398e-03	5.870e-03	4.332e-03	3.089e-03	1.994e-03	1.215e-03
Order	–	0.124	0.438	0.488	0.631	0.714
2^{-21}	6.399e-03	5.868e-03	4.333e-03	3.088e-03	1.995e-03	1.216e-03
Order	–	0.125	0.438	0.489	0.631	0.714
2^{-24}	6.399e-03	5.868e-03	4.333e-03	3.088e-03	1.995e-03	1.216e-03
Order	–	0.125	0.437	0.489	0.631	0.714
2^{-27}	6.399e-03	5.868e-03	4.333e-03	3.088e-03	1.995e-03	1.216e-03
Order	–	0.125	0.437	0.489	0.631	0.714
2^{-30}	6.399e-03	5.868e-03	4.333e-03	3.088e-03	1.995e-03	1.216e-03
Order	–	0.125	0.437	0.489	0.631	0.714
$E^{N,N}$	6.399e-03	5.870e-03	4.333e-03	3.089e-03	1.995e-03	1.216e-03
$Q^{N,N}$	0.125	0.438	0.488	0.631	0.714	–

Table 2: Maximum pointwise error and convergence rate for Z_2 in Example 1 with fixed $\varepsilon_2 = 2^{-6}$

ε_1	$N=16$	$N=32$	$N=64$	$N=128$	$N=256$	$N=512$
Reaction-dominated regime ($\rho\varepsilon_2^2 < \omega\varepsilon_1$)						
2^0	6.430e-06	1.840e-06	5.862e-07	2.239e-07	1.164e-07	6.188e-08
Order	–	1.805	1.650	1.389	0.944	0.911
2^{-3}	9.966e-05	4.084e-05	1.870e-05	9.177e-06	4.576e-06	2.286e-06
Order	–	1.287	1.127	1.027	1.004	1.001
2^{-6}	1.029e-03	4.502e-04	2.001e-04	9.362e-05	4.519e-05	2.219e-05
Order	–	1.192	1.170	1.096	1.051	1.026
Convection-dominated regime ($\rho\varepsilon_2^2 \geq \omega\varepsilon_1$)						
2^{-9}	4.588e-03	3.194e-03	1.680e-03	8.645e-04	4.415e-04	2.229e-04
Order	–	0.522	0.927	0.959	0.969	0.986
2^{-12}	7.133e-03	6.086e-03	4.254e-03	2.935e-03	1.830e-03	1.100e-03
Order	–	0.229	0.517	0.535	0.682	0.733
2^{-15}	8.065e-03	6.684e-03	4.746e-03	3.208e-03	2.023e-03	1.210e-03
Order	–	0.271	0.494	0.565	0.666	0.741
2^{-18}	8.353e-03	6.864e-03	4.951e-03	3.325e-03	2.081e-03	1.245e-03
Order	–	0.283	0.472	0.574	0.676	0.741
2^{-21}	8.396e-03	6.896e-03	4.986e-03	3.345e-03	2.092e-03	1.251e-03
Order	–	0.284	0.468	0.576	0.677	0.742
2^{-24}	8.402e-03	6.900e-03	4.990e-03	3.347e-03	2.094e-03	1.252e-03
Order	–	0.284	0.467	0.576	0.677	0.742
2^{-27}	8.402e-03	6.900e-03	4.991e-03	3.348e-03	2.094e-03	1.252e-03
Order	–	0.284	0.467	0.576	0.677	0.742
2^{-30}	8.402e-03	6.900e-03	4.991e-03	3.348e-03	2.094e-03	1.252e-03
Order	–	0.284	0.467	0.576	0.677	0.742
$E^{N,N}$	8.402e-03	6.900e-03	4.991e-03	3.348e-03	2.094e-03	1.252e-03
$Q^{N,N}$	0.284	0.467	0.576	0.677	0.742	–

Corrected Proof

Table 3: Maximum pointwise error and convergence rate for Z_1 in Example 1 with fixed $\varepsilon_1 = 2^{-18}$

ε_2	$N=16$	$N=32$	$N=64$	$N=128$	$N=256$	$N=512$
Convection-dominated regime ($\rho\varepsilon_2^2 \geq \omega\varepsilon_1$)						
2^{0}	3.057e-03	2.476e-03	1.757e-03	1.246e-03	7.956e-04	4.830e-04
Order	–	0.304	0.495	0.495	0.647	0.720
2^{-3}	1.063e-02	8.522e-03	5.981e-03	4.237e-03	2.698e-03	1.637e-03
Order	–	0.320	0.511	0.497	0.651	0.721
2^{-6}	6.398e-03	5.870e-03	4.332e-03	3.089e-03	1.994e-03	1.215e-03
Order	–	0.124	0.438	0.488	0.631	0.714
2^{-9}	7.171e-03	6.024e-03	4.177e-03	2.873e-03	1.862e-03	1.103e-03
Order	–	0.252	0.528	0.540	0.626	0.756
Reaction-dominated regime ($\rho\varepsilon_2^2 < \omega\varepsilon_1$)						
2^{-12}	4.211e-03	2.821e-03	1.540e-03	8.810e-04	4.903e-04	2.722e-04
Order	–	0.578	0.873	0.806	0.846	0.849
2^{-15}	2.724e-03	1.848e-03	7.563e-04	3.175e-04	1.259e-04	5.195e-05
Order	–	0.560	1.289	1.252	1.335	1.277
2^{-18}	2.455e-03	1.657e-03	6.423e-04	2.469e-04	8.487e-05	2.838e-05
Order	–	0.567	1.367	1.379	1.541	1.580
2^{-21}	2.419e-03	1.632e-03	6.277e-04	2.379e-04	7.966e-05	2.551e-05
Order	–	0.568	1.379	1.400	1.578	1.643
2^{-24}	2.415e-03	1.629e-03	6.259e-04	2.368e-04	7.901e-05	2.515e-05
Order	–	0.568	1.380	1.402	1.583	1.652
2^{-27}	2.414e-03	1.629e-03	6.256e-04	2.366e-04	7.893e-05	2.510e-05
Order	–	0.568	1.380	1.403	1.584	1.653
2^{-30}	2.414e-03	1.628e-03	6.256e-04	2.366e-04	7.892e-05	2.510e-05
Order	–	0.568	1.380	1.403	1.584	1.653

Table 4: Maximum pointwise error and convergence rate for Z_2 in Example 1 with fixed $\varepsilon_1 = 2^{-18}$

ε_2	$N=16$	$N=32$	$N=64$	$N=128$	$N=256$	$N=512$
Convection-dominated regime ($\rho\varepsilon_2^2 \geq \omega\varepsilon_1$)						
2^{0}	5.274e-03	3.793e-03	2.693e-03	1.779e-03	1.105e-03	6.561e-04
Order	–	0.476	0.494	0.598	0.687	0.752
2^{-3}	1.202e-02	8.868e-03	6.330e-03	4.159e-03	2.574e-03	1.524e-03
Order	–	0.438	0.486	0.606	0.692	0.756
2^{-6}	8.353e-03	6.864e-03	4.951e-03	3.325e-03	2.081e-03	1.245e-03
Order	–	0.283	0.472	0.574	0.676	0.741
2^{-9}	8.459e-03	8.092e-03	6.639e-03	4.618e-03	2.747e-03	1.606e-03
Order	–	0.064	0.286	0.524	0.750	0.774
Reaction-dominated regime ($\rho\varepsilon_2^2 < \omega\varepsilon_1$)						
2^{-12}	5.143e-03	4.179e-03	2.577e-03	1.366e-03	6.939e-04	3.526e-04
Order	–	0.299	0.698	0.916	0.977	0.977
2^{-15}	3.398e-03	2.891e-03	1.733e-03	7.498e-04	2.853e-04	1.051e-04
Order	–	0.233	0.738	1.209	1.394	1.440
2^{-18}	3.103e-03	2.667e-03	1.586e-03	6.705e-04	2.367e-04	7.854e-05
Order	–	0.219	0.749	1.242	1.502	1.591
2^{-21}	3.065e-03	2.637e-03	1.567e-03	6.602e-04	2.304e-04	7.519e-05
Order	–	0.217	0.751	1.247	1.519	1.616
2^{-24}	3.060e-03	2.634e-03	1.565e-03	6.589e-04	2.296e-04	7.477e-05
Order	–	0.217	0.751	1.248	1.521	1.619
2^{-27}	3.060e-03	2.633e-03	1.564e-03	6.587e-04	2.295e-04	7.472e-05
Order	–	0.217	0.751	1.248	1.521	1.619
2^{-30}	3.060e-03	2.633e-03	1.564e-03	6.587e-04	2.295e-04	7.471e-05
Order	–	0.217	0.751	1.248	1.521	1.619

Corrected Proof

Table 5: Maximum pointwise error and convergence rate for Z_1 in Example 2 with fixed $\varepsilon_2 = 2^{-3}$

ε_1	$N=16$	$N=32$	$N=64$	$N=128$	$N=256$	$N=512$
Reaction-dominated regime ($\rho\varepsilon_2^2 < \omega\varepsilon_1$)						
2^0	1.503e-04	6.389e-05	2.909e-05	1.383e-05	6.736e-06	3.323e-06
Order	–	1.234	1.135	1.073	1.038	1.019
2^{-3}	2.207e-03	1.023e-03	4.900e-04	2.395e-04	1.184e-04	5.884e-05
Order	–	1.110	1.062	1.033	1.017	1.009
Convection-dominated regime ($\rho\varepsilon_2^2 \geq \omega\varepsilon_1$)						
2^{-6}	1.122e-02	6.748e-03	3.768e-03	2.021e-03	1.046e-03	5.329e-04
Order	–	0.734	0.840	0.899	0.950	0.973
2^{-9}	2.056e-02	1.934e-02	1.542e-02	1.069e-02	7.134e-03	4.443e-03
Order	–	0.088	0.327	0.528	0.584	0.683
2^{-12}	2.337e-02	2.103e-02	1.631e-02	1.134e-02	7.506e-03	4.632e-03
Order	–	0.153	0.367	0.524	0.595	0.696
2^{-15}	2.394e-02	2.134e-02	1.647e-02	1.146e-02	7.576e-03	4.672e-03
Order	–	0.165	0.374	0.523	0.597	0.697
2^{-18}	2.416e-02	2.145e-02	1.651e-02	1.148e-02	7.590e-03	4.681e-03
Order	–	0.172	0.378	0.524	0.597	0.697
2^{-21}	2.424e-02	2.149e-02	1.653e-02	1.149e-02	7.594e-03	4.683e-03
Order	–	0.174	0.379	0.524	0.598	0.698
2^{-24}	2.426e-02	2.150e-02	1.654e-02	1.150e-02	7.596e-03	4.683e-03
Order	–	0.174	0.379	0.524	0.598	0.698
2^{-27}	2.427e-02	2.151e-02	1.654e-02	1.150e-02	7.596e-03	4.684e-03
Order	–	0.174	0.379	0.524	0.598	0.698
2^{-30}	2.428e-02	2.151e-02	1.654e-02	1.150e-02	7.597e-03	4.684e-03
Order	–	0.174	0.379	0.524	0.598	0.698
$E^{N,N}$	2.428e-02	2.151e-02	1.654e-02	1.150e-02	7.597e-03	4.684e-03
$Q^{N,N}$	0.174	0.379	0.524	0.598	0.698	–

Table 6: Maximum pointwise error and convergence rate for Z_2 in Example 2 with fixed $\varepsilon_2 = 2^{-3}$

ε_1	$N=16$	$N=32$	$N=64$	$N=128$	$N=256$	$N=512$
Reaction-dominated regime ($\rho\varepsilon_2^2 < \omega\varepsilon_1$)						
2^0	2.241e-04	8.141e-05	3.297e-05	1.455e-05	6.795e-06	3.277e-06
Order	–	1.461	1.304	1.180	1.099	1.052
2^{-3}	2.704e-03	1.232e-03	5.858e-04	2.853e-04	1.407e-04	6.990e-05
Order	–	1.134	1.072	1.038	1.019	1.010
Convection-dominated regime ($\rho\varepsilon_2^2 \geq \omega\varepsilon_1$)						
2^{-6}	1.737e-02	9.934e-03	5.506e-03	2.912e-03	1.500e-03	7.621e-04
Order	–	0.806	0.852	0.919	0.957	0.977
2^{-9}	3.133e-02	3.040e-02	2.448e-02	1.681e-02	1.119e-02	6.957e-03
Order	–	0.043	0.313	0.542	0.587	0.686
2^{-12}	3.762e-02	3.475e-02	2.707e-02	1.886e-02	1.248e-02	7.696e-03
Order	–	0.115	0.360	0.521	0.596	0.697
2^{-15}	3.884e-02	3.563e-02	2.772e-02	1.932e-02	1.279e-02	7.893e-03
Order	–	0.124	0.362	0.520	0.595	0.696
2^{-18}	3.903e-02	3.582e-02	2.789e-02	1.943e-02	1.287e-02	7.947e-03
Order	–	0.124	0.361	0.521	0.594	0.696
2^{-21}	3.907e-02	3.588e-02	2.795e-02	1.946e-02	1.290e-02	7.966e-03
Order	–	0.123	0.360	0.522	0.594	0.695
2^{-24}	3.907e-02	3.590e-02	2.797e-02	1.948e-02	1.291e-02	7.972e-03
Order	–	0.122	0.360	0.522	0.593	0.695
2^{-27}	3.908e-02	3.590e-02	2.798e-02	1.948e-02	1.291e-02	7.975e-03
Order	–	0.122	0.360	0.522	0.593	0.695
2^{-30}	3.908e-02	3.591e-02	2.798e-02	1.948e-02	1.291e-02	7.976e-03
Order	–	0.122	0.360	0.522	0.593	0.695
$E^{N,N}$	3.908e-02	3.591e-02	2.798e-02	1.948e-02	1.291e-02	7.976e-03
$Q^{N,N}$	0.122	0.360	0.522	0.593	0.695	–

Corrected Proof

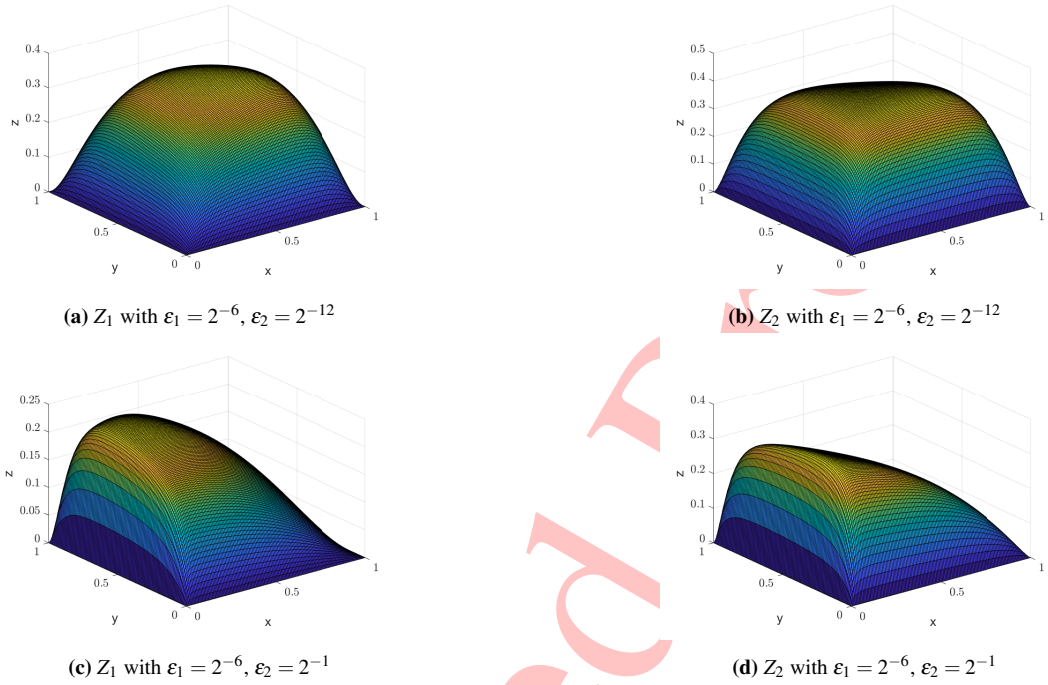

(a) Z_1 with $\varepsilon_1 = 2^{-6}$, $\varepsilon_2 = 2^{-12}$

(b) Z_2 with $\varepsilon_1 = 2^{-6}$, $\varepsilon_2 = 2^{-12}$

(c) Z_1 with $\varepsilon_1 = 2^{-6}$, $\varepsilon_2 = 2^{-1}$

(d) Z_2 with $\varepsilon_1 = 2^{-6}$, $\varepsilon_2 = 2^{-1}$

Figure 3: Surface plots of the numerical solution for Example 2 with $N = 128$: (a), (b) the reaction-dominated regime with $\varepsilon_1 = 2^{-6}$, $\varepsilon_2 = 2^{-12}$; (c), (d) the convection-dominated regime with $\varepsilon_1 = 2^{-6}$, $\varepsilon_2 = 2^{-1}$

Table 7: Comparison of $E^{N,N}$ and $Q^{N,N}$ for the Z_1 component of Example 2 on uniform and Shishkin meshes

Mesh Type		$N = 16$	$N = 32$	$N = 64$	$N = 128$	$N = 256$
Uniform Mesh	$E^{N,N}$	1.840e-02	1.940e-02	1.872e-02	1.675e-02	2.096e-02
	$Q^{N,N}$	-0.077	0.051	0.161	-0.324	–
Shishkin Mesh	$E^{N,N}$	2.428e-02	2.151e-02	1.654e-02	1.150e-02	7.597e-03
	$Q^{N,N}$	0.174	0.379	0.524	0.598	–

scheme on a standard uniform mesh with that on the Shishkin mesh. Figure 6 displays cross-sectional profiles for the solution components Z_1 and Z_2 in Example 2 ($N = 32, \varepsilon_1 = 2^{-12}, \varepsilon_2 = 2^{-3}$). As highlighted in the insets, the uniform mesh does not provide sufficient grid points within the steep boundary layers, resulting in their poor resolution. This is also reflected in the error data. As shown in Table 7, which compares the values of $E^{N,N}$ and $Q^{N,N}$ for the Z_1 component, the errors computed on the uniform mesh do not decrease as N increases, yielding erratic maximum errors and negative convergence rates (e.g., $Q^{N,N} = -0.324$). In contrast, the Shishkin mesh clusters grid points in the layer regions and thereby resolves the singular layers. The computed errors then decrease steadily, as expected from Theorem 2.

Overall, the numerical results obtained for the different parameter combinations are consistent with the theoretical error bounds across the evaluated regimes. As discussed in Remark 1, the observed rates approach two when the convection parameter becomes very small and the problem approaches a reaction-diffusion problem; this is an empirical observation and is not covered by Theorem 2. Within the parameter ranges tested, the computed double-mesh errors behave uniformly in ε_1 and ε_2.

Corrected Proof

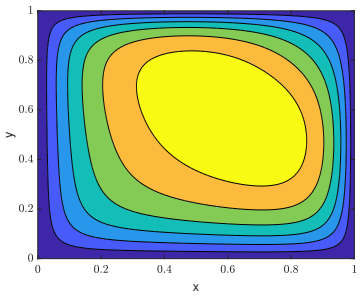

(a) Z_1 with $\varepsilon_1 = 2^{-6}$, $\varepsilon_2 = 2^{-12}$

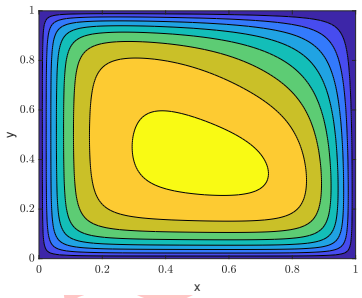

(b) Z_2 with $\varepsilon_1 = 2^{-6}$, $\varepsilon_2 = 2^{-12}$

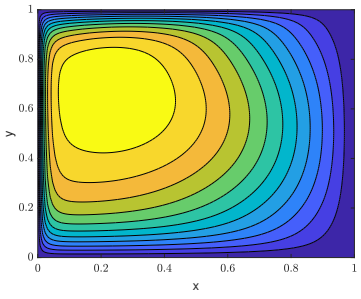

(c) Z_1 with $\varepsilon_1 = 2^{-6}$, $\varepsilon_2 = 2^{-1}$

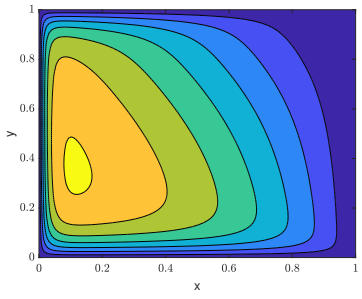

(d) Z_2 with $\varepsilon_1 = 2^{-6}$, $\varepsilon_2 = 2^{-1}$

Figure 4: Contour plots of the numerical solution for Example 2 with $N = 128$: (a), (b) the reaction-dominated regime with $\varepsilon_1 = 2^{-6}$, $\varepsilon_2 = 2^{-12}$; (c), (d) the convection-dominated regime with $\varepsilon_1 = 2^{-6}$, $\varepsilon_2 = 2^{-1}$

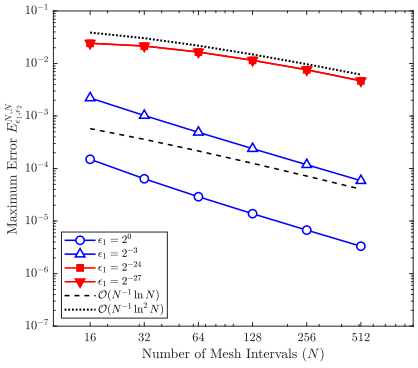

(a) Log–log plot of Z_1

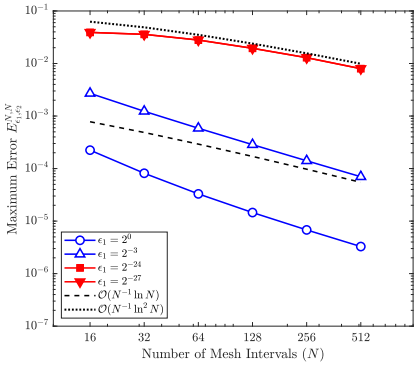

(b) Log–log plot of Z_2

Figure 5: Log–log plots of the maximum pointwise errors for Example 2 with fixed $\varepsilon_2 = 2^{-3}$, mesh resolutions $N = 16, 32, \ldots, 512$, and $\varepsilon_1 \in \{2^0, 2^{-3}, 2^{-24}, 2^{-27}\}$

6 Conclusion

In this paper, a parameter-uniform upwind finite difference scheme has been developed and analyzed for a class of two-parameter singularly perturbed weakly coupled convection-diffusion systems. A piecewise-uniform Shishkin mesh was constructed to resolve the regular, characteristic, and corner layers arising in the solution. The theoretical analysis establishes parameter-uniform convergence of the proposed scheme, with a maximum pointwise error

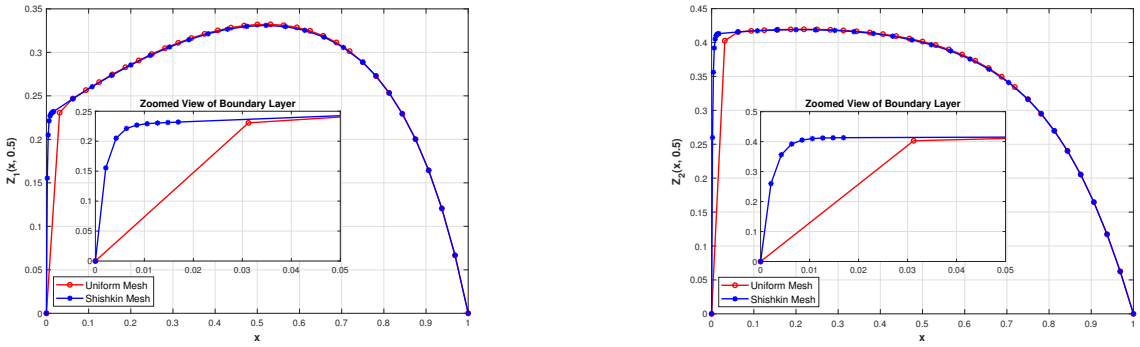

(a) Z_1 cross-section at $y = 0.5$ **(b)** Z_2 cross-section at $y = 0.5$

Figure 6: Comparison of numerical solutions on a uniform mesh versus the Shishkin mesh for Example 2 with $N = 32$, $\varepsilon_1 = 2^{-12}$, and $\varepsilon_2 = 2^{-3}$. The insets highlight the boundary layer region.

of $\mathscr{O}(N^{-1}\ln N)$ in the reaction-dominated regime ($\rho\varepsilon_2^2 < \omega\varepsilon_1$) and $\mathscr{O}(N^{-1}(\ln N)^2)$ in the convection-dominated regime ($\rho\varepsilon_2^2 \geq \omega\varepsilon_1$). The numerical results, with errors estimated by the double-mesh principle, provide evidence consistent with these theoretically proven error estimates. Furthermore, when the convection parameter is sufficiently small, the numerical experiments exhibit an empirical convergence rate approaching second order. We note that this is an empirical observation and is not part of the proven almost first-order parameter-uniform theoretical estimate.

Acknowledgements

The first author extends her gratitude to the Ministry of Education (MoE), Government of India, for its financial assistance.

Declaration of competing interest

The authors have no competing interests to declare that are relevant to the content of this article.

References

[1] M. Brdar, H. Zarin, L. Teofanov, *A singularly perturbed problem with two parameters in two dimensions on graded meshes*, Comput. Math. Appl. **72** (2016) 2582–2603.

[2] H. Chandrasekaran, V. Shanthi, *A computational technique for a 2D singularly perturbed convection-diffusion system with characteristic layers*, Comput. Appl. Math. **45** (2026) 118.

[3] C. Clavero, J.L. Gracia, F. Lisbona, G.I. Shishkin, *A robust method of improved order for convection-diffusion problems in a domain with characteristic boundaries*, ZAMM Z. Angew. Math. Mech. **82** (2002) 631–647.

[4] C. Clavero, R. Shiromani, V. Shanthi, *A numerical approach for a two-parameter singularly perturbed weakly-coupled system of 2-D elliptic convection-reaction-diffusion PDEs*, J. Comput. Appl. Math. **436** (2024) 115422.

Corrected Proof

[5] E.B. Derzie, J.B. Munyakazi, T.G. Dinka, *Parameter-uniform fitted operator method for singularly perturbed Burgers-Huxley equation*, J. Math. Model. **10** (2022) 515–534.

[6] G.F. Duressa, H.G. Debela, *Numerical solution of singularly perturbed differential difference equations with mixed parameters*, J. Math. Model. **9(4)** (2021) 691–705.

[7] T.Y. Ershova, *On the convergence of the Dirichlet grid problem with a singularity for a singularly perturbed convection-diffusion equation*, Moscow Univ. Comput. Math. Cybernet. **40** (2016) 147–154.

[8] P.A. Farrell, A.F. Hegarty, J.J.H. Miller, E. O'Riordan, G.I. Shishkin, *Robust Computational Techniques for Boundary Layers*, Chapman & Hall/CRC, Boca Raton, FL, 2000.

[9] H. Han, R.B. Kellogg, *Differentiability properties of solutions of the equation* $-\varepsilon^2\Delta u + ru = f(x,y)$ *in a square*, SIAM J. Math. Anal. **21** (1990) 394–408.

[10] A.F. Hegarty, E. O'Riordan, *A numerical algorithm to computationally solve the Hemker problem using Shishkin meshes*, J. Comput. Appl. Math. **409** (2022) 114155.

[11] A.F. Hegarty, E. O'Riordan, *A fitted finite element method for singularly perturbed elliptic problems with characteristic boundary layers*, J. Comput. Appl. Math. **474** (2026) 116971.

[12] A.F. Hegarty, E. O'Riordan, *A parameter-uniform upwind finite difference method for a singularly perturbed two parameter elliptic problem with characteristic layers*, Appl. Numer. Math. **231** (2027) 117–134.

[13] P.W. Hemker, *A singularly perturbed model problem for numerical computation*, J. Comput. Appl. Math. **76** (1996) 277–285.

[14] G.J. Jayalakshmi, A. Tamilselvan, *Second order difference scheme for singularly perturbed boundary turning point problems*, J. Math. Model. **9** (2021) 633–643.

[15] R.B. Kellogg, M. Stynes, *Corner singularities and boundary layers in a simple convection-diffusion problem*, J. Differ. Equ. **213** (2005) 81–120.

[16] O.A. Ladyzhenskaya, N.N. Uraltseva, *Linear and Quasilinear Elliptic Equations*, Academic Press, New York, 1968.

[17] J. Li, *A robust finite element method for a singularly perturbed elliptic problem with two small parameters*, Comput. Math. Appl. **36** (1998) 91–110.

[18] J.J.H. Miller, E. O'Riordan, G.I. Shishkin, *Fitted Numerical Methods for Singular Perturbation Problems: Error Estimates in the Maximum Norm for Linear Problems in One and Two Dimensions*, World Scientific Publishing, Hackensack, NJ, revised ed., 2012.

[19] E. O'Riordan, M.L. Pickett, G.I. Shishkin, *Numerical methods for singularly perturbed elliptic problems containing two perturbation parameters*, Math. Model. Anal. **11** (2006) 199–212.

[20] E. O'Riordan, G.I. Shishkin, *Parameter uniform numerical methods for singularly perturbed elliptic problems with parabolic boundary layers*, Appl. Numer. Math. **58** (2008) 1761–1772.

[21] H.-G. Roos, M. Stynes, L. Tobiska, *Robust Numerical Methods for Singularly Perturbed Differential Equations: Convection-Diffusion-Reaction and Flow Problems*, Springer-Verlag, Berlin Heidelberg, second ed., 2008.

[22] L. Teofanov, M. Brdar, S. Franz, H. Zarin, *SDFEM for an elliptic singularly perturbed problem with two parameters*, Calcolo **55** (2018) 50.

[23] L. Teofanov, H.-G. Roos, *An elliptic singularly perturbed problem with two parameters I: Solution decomposition*, J. Comput. Appl. Math. **206** (2007) 1082–1097.

Corrected Proof